Mineralium Deposita
https://doi.org/10.1007/s00126-022-01125-z

ARTICLE

The Black Angel deposit, Greenland: a Paleoproterozoic evaporite-related Mississippi Valley-type Zn–Pb deposit

Diogo Rosa[1] · **David Leach**[2] · **Pierpaolo Guarnieri**[1] · **Andrey Bekker**[3,4]

Received: 28 October 2021 / Accepted: 22 May 2022

Abstract

The Paleoproterozoic Mârmorilik Formation in the Karrat basin of West Greenland hosts the Black Angel Zn–Pb deposit. Chlorine-rich scapolite, zones with vuggy porosity and quartz nodules in the ore-bearing marble are herein interpreted to represent metamorphosed, vanished, and replaced evaporites, respectively. Mineralization is closely associated with anhydrite with $\delta^{34}S$ values (5.2–12.6‰) broadly comparable to published values for Paleoproterozoic seawater sulfate. Considering the fundamental attributes of the mineralization and host sequence, a Mississippi Valley-type (MVT) model is the most obvious explanation for mineralization. Overlying the ore-bearing sequence are organic-rich semipelites and massive calcitic marbles, which may have served as seals for hydrocarbon or reduced sulfur and acted as chemical traps for deposition of the sulfidic ore. The Mârmorilik Formation contained an interlayered sulfate-rich evaporite-carbonate sequence, a common setting for MVT deposits in the late Neoproterozoic and Phanerozoic, but unique among the few known MVT deposits in the Paleoproterozoic. This ca. 1915 Ma evaporite-carbonate platform is younger than sulfate evaporites deposited during and immediately after the ca. 2220–2060 Ma Lomagundi carbon isotope excursion and records a significant seawater sulfate level during a time interval when it was assumed that it had been too low to form extensive evaporite deposits. Therefore, MVT and clastic-dominated (CD) Zn–Pb deposits in the geological record might progressively fill the apparent gap in marine sulfate evaporites and provide unique insights into Proterozoic seawater sulfate level. Considering the sequence of tectonic events that affected the Karrat basin, the mineralization took place between Nagssugtoqidian collision (< 1860 Ma) and Rinkian metamorphism (ca. 1830 Ma).

Keywords MVT Zn–Pb deposits · Paleoproterozoic · Evaporites · Greenland · Paleoproterozoic seawater sulfate level

Introduction

The Black Angel deposit on the West coast of Greenland (Fig. 1) is a significant Zn–Pb deposit hosted in the Paleoproterozoic Mârmorilik Formation, with pre-mining reserves of 13 Mt, at 12% Zn, 4% Pb, and 29 ppm Ag (Thomassen 1991). The deposit encompasses eight different ore bodies and two satellite ore bodies (the Nunngarut orebodies) located ca. 4 km to the southwest (Fig. 2). Outcropping mineralized occurrences occur in similar settings, 4–10 km to the southeast and approximately 85 km to the southwest of Black Angel. The stratabound ore bodies are hosted in anhydrite-bearing marble and consist of massive to semi-massive sphalerite-galena-pyrite, with minor to trace amounts of chalcopyrite, arsenopyrite, tetrahedrite, freibergite, tennantite, stannite, briartite, enargite, loellingite, polybasite, magnetite, rutile, and graphite (Pedersen 1980; Horn et al. 2019). The abundance of pyrite, with massive

Editorial handling: Karen Kelley

✉ Diogo Rosa
dro@geus.dk

[1] Department of Mapping and Mineral Resources, Geological Survey of Denmark and Greenland (GEUS), Copenhagen 1350, Denmark

[2] Center for Mineral Resources Science, Department of Geology and Geological Engineering, Colorado School of Mines, Golden, CO 80401, USA

[3] Department of Earth and Planetary Sciences, University of California, Riverside, CA 92521, USA

[4] Department of Geology, University of Johannesburg, Johannesburg 2092, South Africa

Published online: 03 June 2022

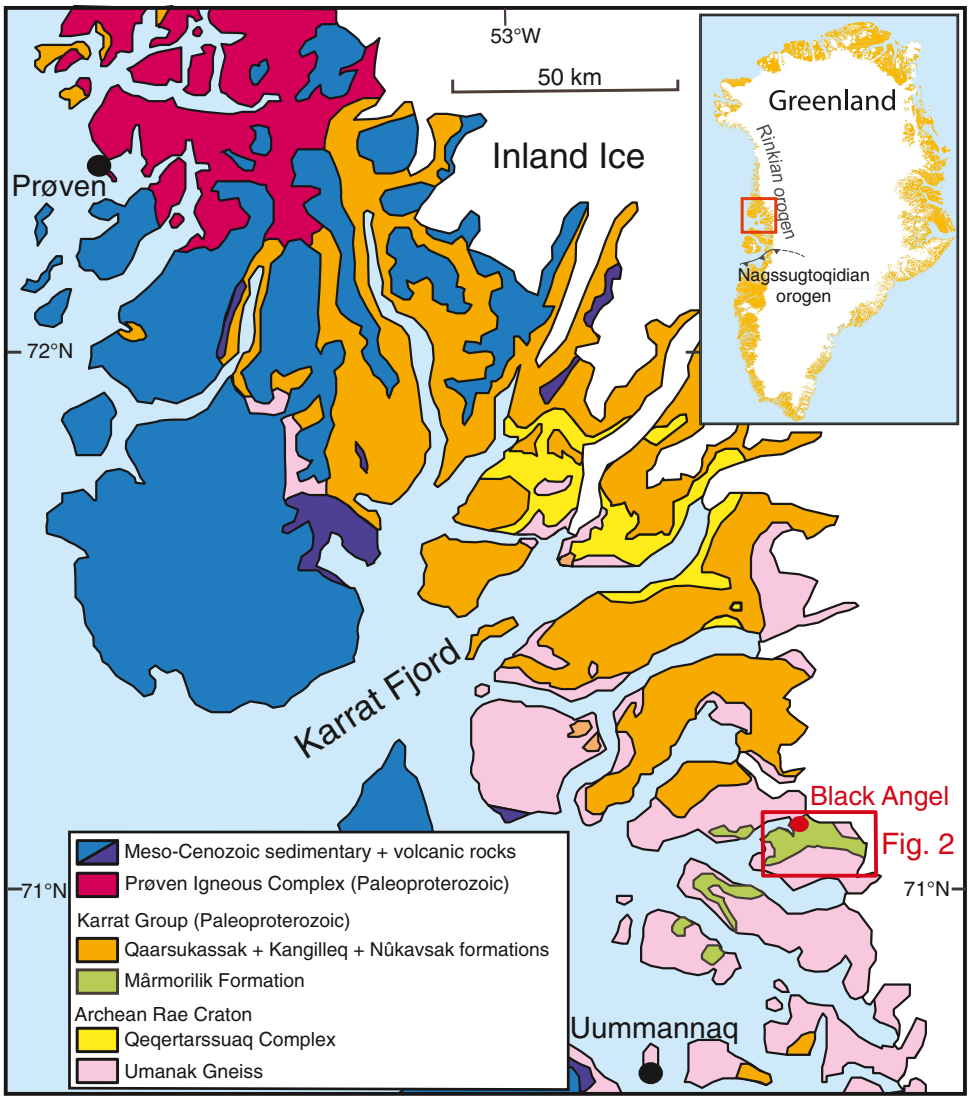

Fig. 1 Regional location showing distribution of the Karrat Group in West Greenland, including the Mârmorilik Formation, host for the Black Angel deposit. Red rectangle indicates the location of the Maarmorilik area and the Black Angel deposit, shown in detail in Fig. 2

sulfide zones of the Angel and Cover orebodies containing 42 vol % pyrite, is unusual for most carbonate-hosted –-Pb deposits. In addition to its economic importance, attested by active underground mining between 1973 and 1990, the Black Angel deposit is noteworthy for being one of the few known non-magmatic Zn–Pb deposits hosted in Paleoproterozoic carbonate rocks (Leach et al. 2005, 2010; Kesler and Reich 2006).

Despite the long mining and exploration history, the genesis of this deposit remains debated. This can be attributed to the effect of greenschist facies metamorphism and intense multi-stage deformation that affected and remobilized the ore (Pedersen 1980, 1981). The deposit has been classified as an exhalative sediment-hosted massive sulfide deposit by some workers (SEDEX; Sangster 1990; Leach et al. 2005). Note that the term "SEDEX" is only used in this report for citations to historical publications, the CD term is the preferred term for clastic-dominated (CD) Zn–Pb deposits as per the usage described in Leach et al. 2010. Other workers classify the Black Angel deposit as an epigenetic Mississippi Valley-type (MVT) deposit (Carmichael 1988; Kolb et al. 2016; Rosa et al. 2017; Partin et al. 2021). Horn et al. (2019) disputed a MVT and SEDEX classification and favored a metamorphic Kipushi-style model.

We examined publications and field reports on the Black Angel deposit to provide insights into the genesis of the mineralization, and we evaluated the origin of the Black Angel deposit based on recent advances in the understanding of sediment-hosted deposits. Newly acquired structural data constrain the timing of mineralization and deformation within a context of the evolving Paleoproterozoic Nagssugtoqidian and the Rinkian orogens. Additional field observations and limited new analytical results reveal a close association of mineralization with anhydrite in a shallow-marine carbonate platform sequence containing extensive meta-evaporites and vanished evaporites. The important

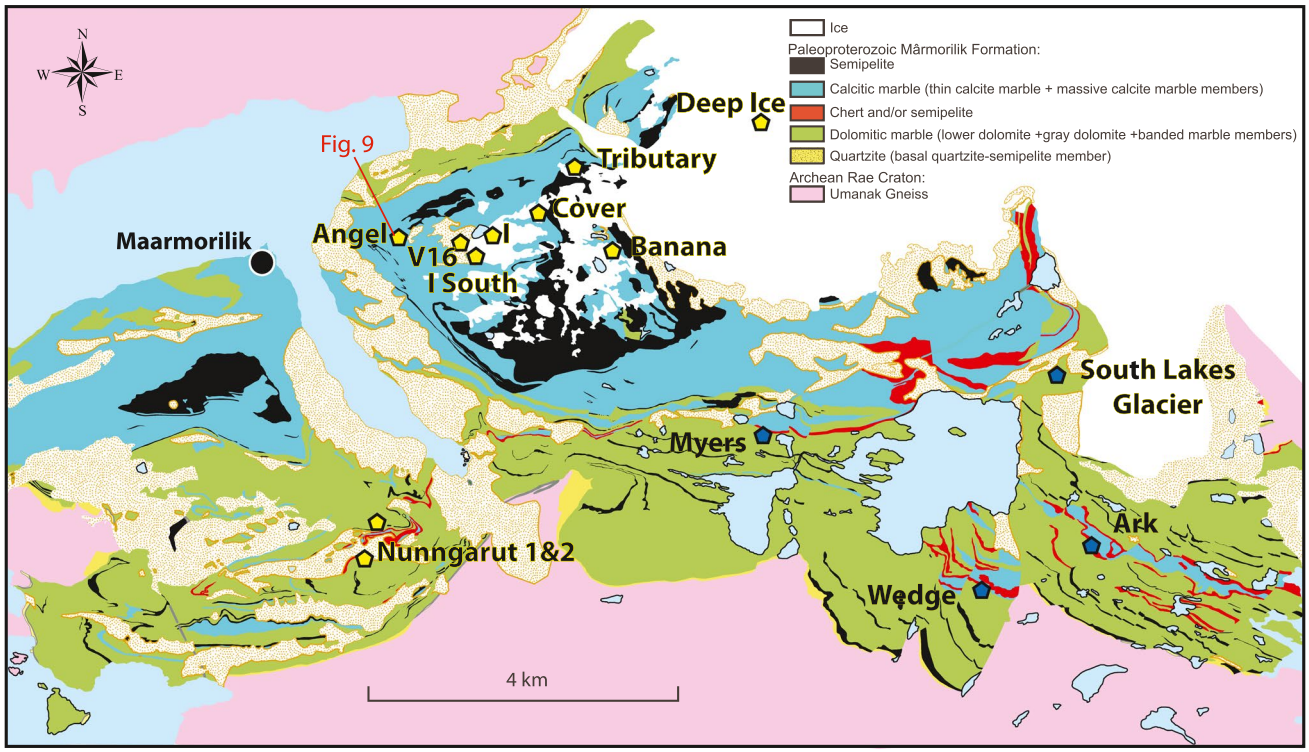

Fig. 2 Geological map of the Maarmorilik area based on Garde (1978) and King (1983). Blue pentagons show outcropping mineral occurrences in dolomitic marbles and yellow pentagons correspond to surface projection of subsurface orebodies of the Black Angel deposit (including its satellite Nunngarut orebodies). Location of Fig. 9 is also shown

association between mineralization and evaporites presented here has been underappreciated for the Mârmorilik Formation, perhaps due to the elusive nature of evaporites in the rock record of this unit and the middle Paleoproterozoic worldwide. Automated mineralogy and electron probe microanalysis (EPMA) were conducted on one sample (five new analyses) of scapolite-bearing marble from surface outcrops to determine the content of Na, Ca, and Cl in scapolite to resolve whether it is related to an evaporite-bearing protolith. The S isotopic composition of two underground samples (five analyses) of anhydrite from the GEUS' archive allows a rare glimpse into the isotopic composition of the middle Paleoproterozoic seawater sulfate.

Regional geological setting

The middle Paleoproterozoic Karrat Group (Fig. 1) is an approximately 8.5-km-thick metasedimentary sequence, deposited after ca. 2000 Ma (Kalsbeek et al. 1998), which unconformably overlies the Archean Umanak Gneiss Complex in northern West Greenland (Henderson and Pulvertaft 1967, 1987). According to Henderson and Pulvertaft (1987), the Karrat Group includes the lower (mainly siliciclastic) Qeqertarssuaq Formation, the carbonate-dominated Mârmorilik Formation, and the upper turbiditic Nûkavsak Formation that locally contains pyrrhotite-chert-graphite horizons. Intercalated within the lower part of the Nûkavsak Formation, there are mafic metavolcanic rocks, which were recently given formation status in the published geological maps: the Kangilleq Formation (Guarnieri et al. 2022a). Furthermore, on these maps, the Qeqertarssuaq Complex (previously called the Qeqertarssuaq Formation) is removed from the Karrat Group and included in the Archean gneiss complexes. Instead, the siliciclastic-dominated Qaarsukassak Formation has been defined as the base of the Karrat Group in the central area of Fig. 1, and is therefore correlative to the basal part of the Mârmorilik Formation (Guarnieri et al. 2016; 2022b).

Inversion of the Karrat basin occurred during the collision between the Archean Rae craton and the Meta Incognita microcontinent during the Trans-Hudson Orogeny (St-Onge et al. 2009). The Karrat Group rocks were involved in the Rinkian fold-and-thrust belt deformation and their metamorphic grade decreases from granulite facies, near the Prøven Igneous Complex in the NW, to greenschist facies, towards the Maarmorilik area to the SE (Fig. 1). The earlier Rinkian deformation (with vergence to the present east) was thin skinned whereas the later Rinkian deformation was associated with thick-skinned thrusting to the present northeast

(Rosa et al. 2018). The Rinkian Orogen is related to subduction and calc-alkaline magmatism between 1900 and 1850 Ma (Guarnieri et al. 2022c). Peak metamorphism, with migmatization during collision, is constrained by S-type leucogranite magmatism at ca. 1830 Ma (Guarnieri et al. 2022d) and the 1826 ± 9 Ma U–Pb reset apatite age for the Karrat Group metavolcanic rocks (Kirkland et al. 2017).

Approximately 150 km towards the present-day south, the Rae and North Atlantic craton collided, which resulted in the Nagssugtoqidian Orogeny (see inset in Fig. 1) with deformation extending to the southernmost part of the Karrat area (Grocott and McCaffrey 2017). The tectonic history of the Nagssugtoqidian Orogeny includes subduction and calc-alkaline magmatism between 1920 and 1870 Ma (Kalsbeek et al. 1987). Peak metamorphism occurred during collision at ca. 1850 Ma (Kalsbeek et al. 1987), which was followed by later N-S shortening with folding dated at ca. 1825 Ma and subsequent strike-slip movement with associated folding at ca. 1775 Ma (Connelly et al. 2000). In summary, the Nagssugtoqidian and Rinkian orogenies broadly overlapped both temporally and spatially, at their fronts, throughout a sequence of events lasting for approximately 150 million years.

District geology

The Black Angel deposit and associated smaller occurrences (Fig. 2) are hosted by the Mârmorilik Formation in the southern part of the Karrat area (Fig. 1). This shallow-water, stromatolite-bearing marine carbonate platform (Pedersen 1978) extended for at least 85 km to the SW of Maarmorilik. This unit was originally considered to be Archean in age (Henderson and Pulvertaft, 1967), but the identification of an angular unconformity with the underlying Umanak Gneiss led to its inclusion in the Karrat Group (Garde and Pulvertaft 1976; Henderson and Pulvertaft 1987). The maximum depositional age of the Mârmorilik Formation is constrained by detrital zircon U–Pb geochronology (Fig. 3). Quartzites of the basal part of the Mârmorilik Formation, correlative to the Qaarsukassak Formation, define the maximum depositional age of ca. 2000 Ma, whereas pelites intercalated with marbles of the Mârmorilik Formation provide the maximum depositional age of ca. 1915 Ma (Guarnieri et al. 2022b). A Pb–Pb age of 1881 ± 20 Ma for a marble of the Mârmorilik Formation (Taylor and Kalsbeek, 1990), originally considered as a metamorphic age, is here re-interpreted as a diagenetic age based on the fact that the Rinkian metamorphism has been dated at ca. 1830 Ma (Kirkland et al 2017; Guarnieri et al. 2022d) and the Nagssugtoqidian metamorphism was dated at ca. 1850 Ma (Kalsbeek et al. 1987). Therefore, the age from Taylor and Kalsbeek (1990) is much older than the known metamorphic events. Moreover, it has been shown that U–Pb systematics of marble can preserve diagenetic ages under greenschist facies conditions (Bolhar et al. 2002; Ovchinnikova et al. 2007). As such, the age reported by Taylor and Kalsbeek (1990) provides a minimum age for the Mârmorilik Formation.

A basal quartzite-semipelite member, which consists of orthoquartzite and overlying quartzite interbedded with calcsilicates and semipelite, is overlain by the lower dolomite member, which consists of impure quartz- and tremolite-bearing dolomitic marble, and pure dolomitic marbles (Garde 1978; King 1983; Figs. 2 and 3). The Nunngarut orebodies and the Ark and Wedge showings are hosted by the lower dolomite member (Fig. 2). This member is overlain by the thin calcite marble member, which consists of fine- to medium-grained, phlogopite-bearing calcitic marble with bands of chert and semipelite. The overlying grey dolomite member is massive, homogeneous, phlogopite-, pyrite-, and graphite-bearing dolomitic marble. These members are succeeded by the banded marble member with chert and semipelite bands and quartz-bearing dolomitic marble, hosting the South Lakes Glacier and Myers showings. Above this member is the massive calcite marble member of phlogopite-bearing calcitic marble, which, in the proximity of the Black Angel deposit, becomes more dolomitic and anhydrite and graphite rich (Pedersen 1980). According to Garde (1978), these marble members are overlain by the laminated semipelite member (Fig. 3). Garde (1978) reported that graphite is common in the Mârmorilik Formation, with several samples yielding approximately 1% graphite.

A more detailed stratigraphy was established by Cominco geologists for the part of the massive calcite marble member hosting the Black Angel deposit (inset in Fig. 3; Nichols 1984; Harris 1986). These authors describe a "footwall sequence" in the folded stratabound orebody consisting of massive, anhydritic (up to 2–20% anhydrite), white, dolomitic marble, and an "ore-bearing sequence" with dolomitic marble alternating in color from white to grey and having up to 11% porosity. The zones of vuggy and porous marbles were interpreted to reflect dissolved evaporite minerals (Harris 1986) or "vanished" evaporites (cf. Warren 2016). The vuggy porosity is likely a very late feature produced by the dissolution of the sulfates by infiltrating meteoric water during uplift. Zones of dolomitic marble commonly contain quartz nodules and quartz "eyes" that could reflect silicified gypsum/anhydrite, common in diagenetically altered evaporite-bearing carbonates (e.g., Chown and Elkins 1974; Warren 2016; Leach and Song 2019). Above the ore zone is a "lower hanging wall sequence" of white to light-grey, mica-bearing, banded calcitic, and quartzitic marbles with up to 40% of quartz blebs and nodules and an "upper hanging wall sequence" of graphitic, cherty, and pyritic/pyrrhotitic pelites,,transitional to the semipelite member of Garde (1978).

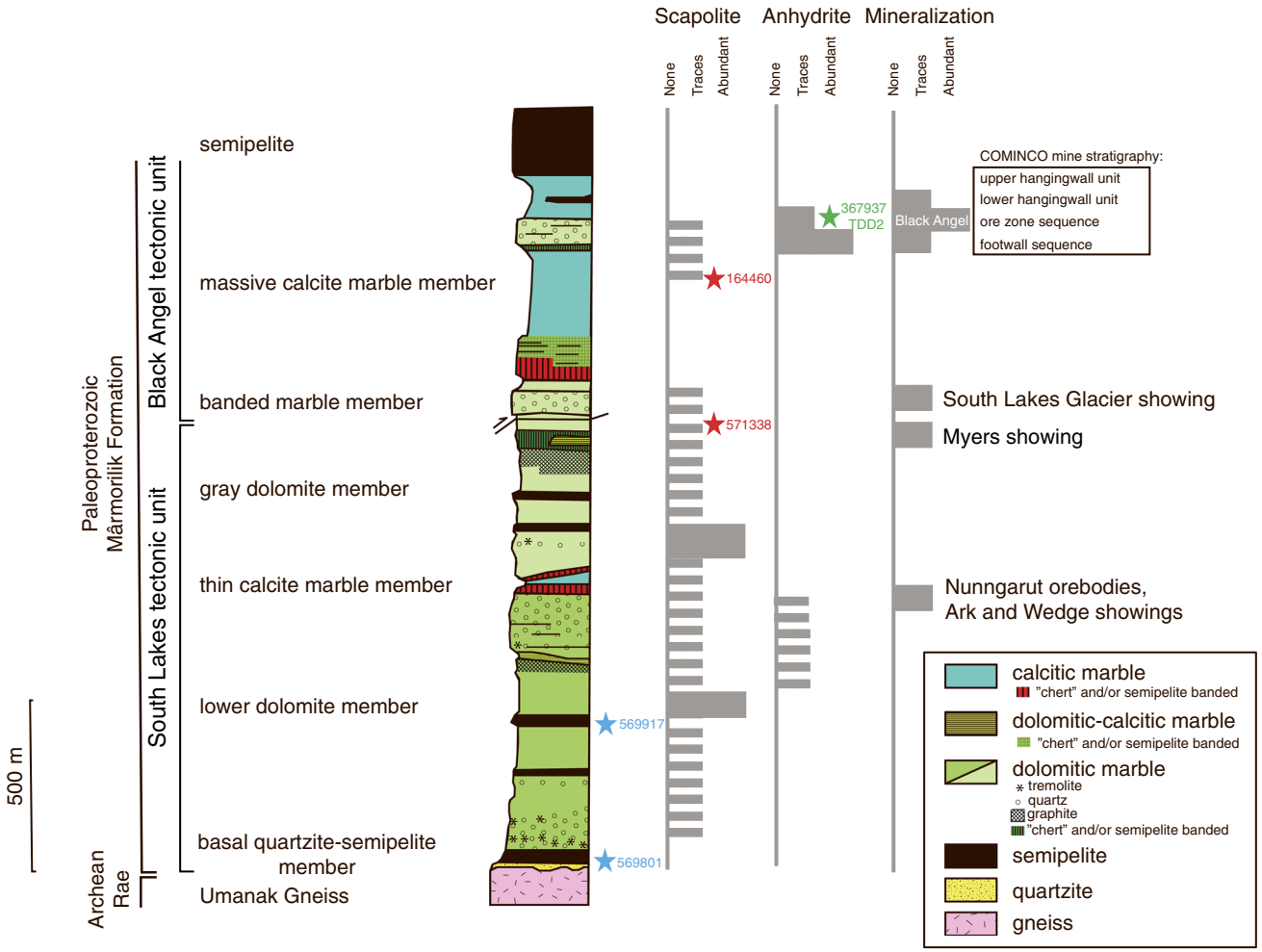

Fig. 3 Generalized stratigraphic column of the Mârmorilik Formation (modified after Garde 1978). Section is likely structurally repeated as discussed in the text. Variations in scapolite, anhydrite, and ore contents (none, traces (~1%), abundant (~5% or more)) were established from field observations and Garde (1978), King (1983), Nichols (1984), and Harris (1986). Locally, anhydrite can reach up to 20 vol % in meter-thick bands. Blue stars mark siliciclastic samples that were characterized with U–Pb zircon geochronology (Guarnieri et al. 2022b), providing Maximum Depositional Ages (MDA); quartzite of the Qaarsukassak Formation (sample 569,801; MDA of ca. 2000 Ma) correlative to the Mârmorilik Formation basal siliciclastic rocks; pelites intercalated with marbles (sample 569,917, MDA of ca. 1915 Ma). Red stars correspond to scapolite samples 164,460, analyzed by Garde (1978), and 571,338, analyzed as part of this study. Green star marks the position of anhydrite samples analyzed for S isotope composition (this study). Also shown is the distribution of graphite, tremolite, and quartz

Whereas the ore bodies in the Black Angel deposit are overlain by calcitic marble and thick graphitic semipelites, occurrences in the lower part of the Mârmorilik Formation are located immediately below other distinct stratigraphic levels (Figs. 2 and 3), designated as "chert and/or semipelite" by Garde (1978) or as "cherty and mottled pelite" by King (1983). As shown in Figs. 2 and 3, these levels mark the contact between dolomitic and calcitic marble members. In the field, these levels were recognized as clast-supported monomictic breccia with siliceous pelitic clasts cemented by calcite (Fig. 4). Garde (1978) and King (1983) interpreted this monomictic breccia, controlling mineralization in the lower part of the Mârmorilik Formation, as a shear contact. However, this breccia does not display any tectonic fabric. Henderson and Pulvertaft (1987) considered that the transition from a more dolomitic lower part to a more calcitic upper part of the Mârmorilik Formation reflects a marine transgression. Guarnieri and Baker (2022) considered that the transition from dolomitic to calcitic marble broadly defines two tectonic units (South Lakes tectonic unit and Black Angel tectonic unit, respectively), which are separated by a thrust within gray dolomitic marbles, below the monomictic breccia. This interpretation places the South Lakes Glacier occurrence within the Black Angel tectonic unit, even if it is hosted within dolomitic marbles. As such, this occurrence can be seen as a tectonostratigraphic analog

Fig. 4 Clast-supported monomictic breccia, with siliceous pelitic clasts cemented by calcite, displaying no tectonic fabric. South Lakes, Maarmorilik area. This unit is approximately 2 m thick. We suggest this and similar horizons may have acted as stratigraphic traps for hydrocarbons or reduced sulfur fluids

to the succession hosting the Black Angel deposit. Another implication of this interpretation is that thrusting would have significantly thickened the carbonate sequence and thus Fig. 3 does not represent the original stratigraphic thickness. Thrusting could have also contributed to the more deformed nature of the Black Angel tectonic unit relative to the South Lakes tectonic unit.

The folding that affected the lower part of the Mârmorilik Formation produced repetition of the dolomitic marble sequence. Consequently, the lower dolomite and gray dolomite members, plus the banded marble member, represent the same stratigraphic package that is repeated at two limbs of a fold with the thin calcite marble member in its core (Fig. 3).

Mârmorilik-mixed evaporite-carbonate platform

Wave ripples and crossbedding in quartzites of the basal quartzite-semipelite member suggest that deposition of the Mârmorilik Formation started in a shallow-water, high-energy environment, followed by fine-grained sediments, consistent with deepening and finally, as the supply of detrital material decreased, an extensive carbonate platform developed (Henderson and Pulvertaft 1987). Subsequently, the platform was rapidly drowned, with the establishment of a deep and sediment-starved basin which was buried by turbidites of the Nûkavsak Formation (Guarnieri et al. 2022b; 2022e).

Despite repetition along a few discrete sheared contacts, as documented above, the Mârmorilik Formation stratigraphy mostly reflects deepening of the depositional environment from a carbonate platform with widespread evaporite deposition to a deeper-water marine setting.

Anhydrite in the Mârmorilik Formation

Based on the observations of our study, drill hole logs, and previous studies, the distribution and relative abundance of anhydrite are illustrated in the generalized stratigraphic column of Fig. 3. There is no evidence for zoning in anhydrite nor is there evidence for secondary Zn silicates or carbonates in the host rocks that could develop by the oxidation of sulfides during weathering. Calcium sulfate rarely occurs in primary MVT ore assemblages, but can be produced by the dissolution of Ca carbonates in a sulfate-rich ore fluid. If this occurred at the Black Angel deposit, a zoning of anhydrite related to the intensity of carbonate replacement during mineralization would develop, which has not been observed. Therefore, we infer that anhydrite reflects sedimentary sulfate evaporite (cf. McKibben et al. 1988), which was part of the original sedimentary sequence. Archived samples stored at GEUS reveal that anhydrite occurs in these marbles as lilac-colored patches (Fig. 5a). The anhydritic marbles are well documented in mine logs and cross sections (Garde 1978; Harris 1986; Nichols 1984). For example, Harris (1986) states that the footwall of the Black Angel deposit contains a thick sequence of massive, white dolomitic marble, which contains 2–20% of anhydrite in thin bands, pods, and lenses, elongated parallel to foliation. Disseminated anhydrite also occurs in dolomitic marbles of the lower part of the Mârmorilik Formation (Harris 1985), but it is generally less abundant relative to the host rocks for the Black Angel deposit.

There are no thick, layered evaporites preserved in the Mârmorilik Formation. Evaporite minerals (halite, anhydrite, gypsum) can be removed from the rock record through dissolution, diagenesis, and halokinesis. Diagenetic replacement of gypsum/anhydrite by calcite or silica is well documented (Chown and Elkins 1974; Pierre and Rouchy 1988; Dejonghe et al. 1998; Sanz-Rubio et al. 2001; Hanor, 2004; Stafford et al. 2008). Intense deformation and metamorphism of the Mârmorilik Formation would have destroyed massive layers of halite and anhydrite due to difference in rheological properties from those of their host rocks. The halokinetic migration of layered evaporites to shallow or surface locations during burial or deformation is extensively described (e.g., Hudec and Jackson 2006, 2007; Warren 2016 and references therein). In the Mârmorilik Formation, anhydrite (formerly gypsum) that survived deformation and metamorphism has not been identified in outcrops because it would have been dissolved when exposed to surface conditions when Greenland was positioned in a warmer and wetter climatic zone. These surviving masses of anhydrite in the Black Angel

Fig. 5 Evidence for evaporite and meta-evaporites in the Mârmorilik Formation: **a** marble with lilac-colored patches of anhydrite and scapolite (sample 367,937, Deep Ice orebody, Black Angel deposit); **b** euhedral scapolite crystals in outcrop of a dolomitic marble (sample 571,338, South Lakes Glacier occurrence, lower part of the Mârmorilik Formation)

deposit are in cores of recumbent folds that were likely areas of lower stress and were less susceptible to halokinetic migration. Therefore, the present masses of anhydrite in the marbles of the Black Angel deposit must be considered as "survivors" of a more extensive evaporite sequence that was likely dominated by halite. A comparable occurrence of sedimentary anhydrite is preserved in the Mesoproterozoic (1300 to 1150 Ma) Balmat deposit, New York (Whelan et al. 1990; Corriveau et al. 2007), that experienced amphibolite grade metamorphism and deformation. Another illustration of surviving masses of anhydrite is the ca. 2100 Ma evaporite-carbonate succession in the Onega basin of Karelia, Russia, where evaporites were not suspected based on outcrop observations (except for saline groundwaters), but shallow- to intermediate-depth drilling documented collapse breccias and pseudomorphs after gypsum and halite, and deep-level drilling accidentally penetrated a salt diapir in which a thick sequence of sulfate and halite was preserved (Morozov et al. 2010).

The S isotope values (see Methods in Online Resources 1) of five analyzed sub-samples of anhydrite from the Black Angel deposit cluster in two distinct sets (Table 1 in Online Resource 2): 5.2, 5.3, and 5.6‰ from the Angel orebody (sample TDD2), and 10.9 and 12.6‰ from drift 216 in the Deep Ice orebody (sample 367,937, Fig. 5a). These orebodies, as other Black Angel deposit orebodies, are hosted by the same stratigraphic interval (Fig. 3). It is difficult to equate the anhydrite S isotope values directly to the Paleoproterozoic seawater sulfate composition due to the unknown extent of evaporation that likely occurred on the Mârmorilik-mixed evaporite-carbonate platform. Variable amounts of seawater evaporation can shift sulfate evaporites to slightly heavier S isotope values. The isotopic shift related to seawater evaporation is less than + 2‰ for gypsum

precipitation based on experiments and theoretical considerations; however, the typical change in S isotope values of sulfate evaporites due to their precipitation is much smaller and negligible (Thode and Monster, 1965). Therefore, the difference between the two sets of data is unlikely to be reconciled by the different extent of evaporation. The modern seawater sulfate residence time is ~ 20 million years (Yao et al. 2019) and, as a result, modern to late Phanerozoic sulfate evaporites typically show small stratigraphic $\delta^{34}S$ variations, except for short time periods with low and variable seawater sulfate content. However, between the Lomagundi Event at ca. 2220–2060 Ma and ca. 810 Ma, stratigraphic $\delta^{34}S$ variations in sulfate evaporites and carbonate-associated sulfate (CAS) were much larger (Kah et al. 2004; Planavsky et al. 2012; Turner and Bekker 2016; Crockford et al. 2019), and are consistent with the range of values observed in this study. There are strikingly few $\delta^{34}S$ data available for shallow-marine sulfate evaporites and CAS for the mid-Proterozoic with only the ca. 1.89 Ga Tadpatri Formation from the Cuddapah basin of Eastern India being roughly similar age to the Mârmorilik Formation (Fig. 6). The Tadpatri Formation gypsum shows a range of $\delta^{34}S$ values from + 19.0 to + 23.3‰ ($n = 5$; Crockford et al. 2019), which are higher than those in our study. An alternative and indirect estimate for seawater composition is provided by sulfates (anhydrite, gypsum, and barite) associated with the ca. 1.9–1.8 Ga volcanogenic massive sulfide deposits at Anderson Lake (MB, Canada; Walford and Franklin 1982), Agucha Zn–Pb mine (Rajasthan, India; Fareeduddin et al. 2014), and Åsen and Falun (Sweden; Gavelin et al. 1960; Rickard et al. 1979) that have $\delta^{34}S$ values ranging from + 1.5 to + 15.0‰ (Fig. 6). Five sulfur isotope values for sulfate in our study overlap with this range; however, contribution of volcanic sulfur to this range of values could have compromised the seawater signature. The Black Angel sulfate $\delta^{34}S$ values also overlap with the range of S isotope values for sulfate evaporites deposited in shallow-marine environments during the older ca. 2220–2060 Ma Lomagundi carbon isotope excursion worldwide (see Fig. 6; Bekker et al. 2006; Schröder et al. 2008; Planavsky et al. 2012; Crockford et al. 2019).

Meta-evaporite minerals of the Mârmorilik Formation

Evidence for former evaporites in the Mârmorilik Formation includes the widespread occurrences of Cl-rich scapolite (Garde 1978) and albite, which are the products of metamorphism of sedimentary sequences containing evaporites, carbonates and plagioclase (e.g., Serdyuchenko 1975; Hogarth and Griffin 1978; Moine et al. 1981; Mora and Valley 1989; Gomez-Pugnaire et al. 1994; Warren 2016 and references therein).The distribution and abundance of scapolite are illustrated in the generalized stratigraphic column of Fig. 3. Scapolite is common in anhydritic marbles in the Black Angel deposit (Fig. 5a) and in outcrops of dolomitic marbles of the lower part of the Mârmorilik Formation (Fig. 5b). According to Garde (1978) and our own limited analytical results for the scapolite crystals shown in Fig. 7, scapolite contains 2.4–2.7% Cl and is the Na-rich marialite endmember (Table 2 in Online Resource 3).

Albite is widely present and is reported as an accessory or minor phase by Garde (1978) in the lower dolomite member, gray dolomite member, banded marble member, and massive calcite member marbles and as a significant phase in the semipelite member. Some of the albite in marbles co-occurs with quartz, calcite, and chlorite, which form pseudomorphs after scapolite and may represent a late fluid event. The processes involved in albitization are discussed in detail by Warren (2016) and references therein. Warren (2016) states that considering that "most scapolite forms via the metamorphic alteration of plagioclase feldspar by Na-rich fluids, consequently albitization and scapolitization are typically co-associated metamorphic outcomes." The extensive interlayered scapolite and albite in the regionally

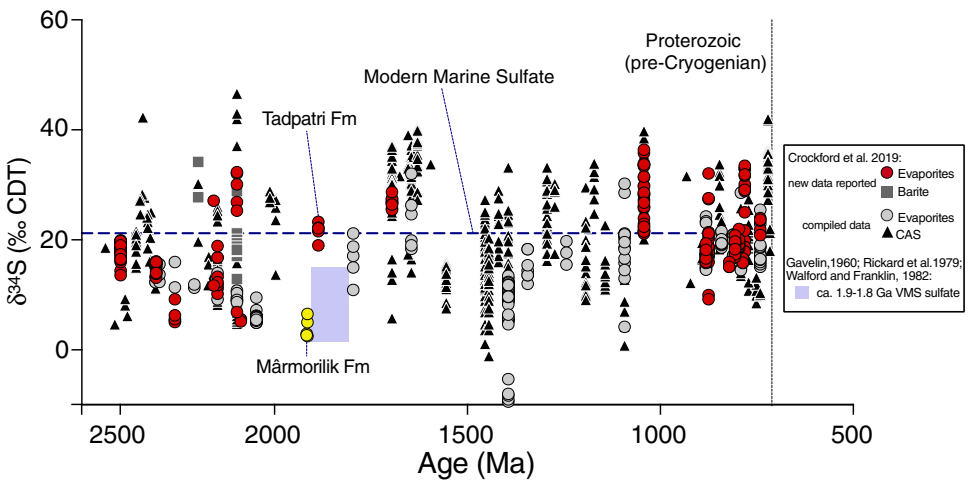

Fig. 6 Secular seawater-sulfate S isotope record modified after Crockford et al. 2019 (including literature data compiled in their study). Yellow circles show $\delta^{34}S$ data for the Black Angel deposit sulfate and blue rectangle shows the range of $\delta.^{34}S$ values for sulfate associated with the ca. 1.9–1.8 Ga volcanogenic massive sulfide deposits (from Gavelin et al. 1960; Rickard et al. 1979; Walford and Franklin 1982)

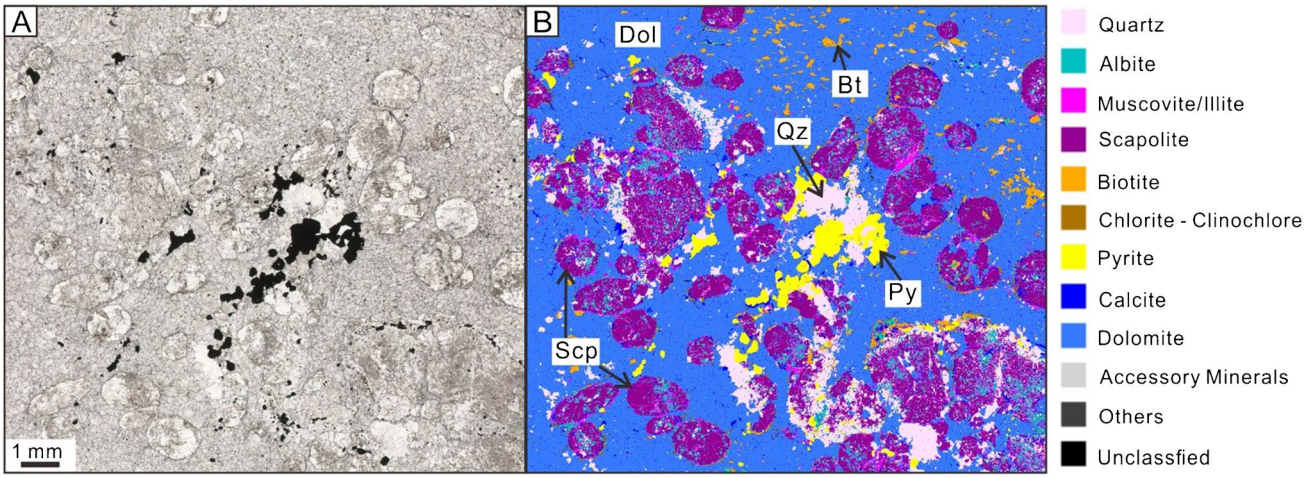

Fig. 7 **a** Transmitted light photograph and **b** mineralogical map from automated SEM (TESCAN) of sample 571,338 (dolomitic marble) from the lower part of the Mârmorilik Formation. Note the presence of scapolite, a sodium-rich (marialite) variety with about 2.5% Cl (see Table 2, Online Resource 3)

metamorphosed sequence therefore argue for the presence of former evaporite units rather than a local skarn or hydrothermal system (cf. Warren 2016). A skarn or any other type of magmatic hydrothermal product would likely be associated with local alteration phases along faults and fractures and a zoned alteration pattern that are absent in the Black Angel district. This is also consistent with the absence of Paleoproterozoic intrusions in the Maarmorilik area.

Deformation and structures

Pedersen (1980; 1981) described the effects of greenschist metamorphism and deformation on the morphology of the ore bodies which had an original thickness, prior to deformation, of between 0.5 to 8 m, and on sulfide ore textures. These events created ore zones that conform to the deformation and metamorphic fabrics and structures (Fig. 8). Shear deformation resulted in the syntectonic recrystallization and ductile transport of sphalerite and galena from high strain areas (fold limbs) to low strain areas (fold hinges and fractures) as illustrated in Fig. 8. Original paragenetic relationships were compromised and ore textures were dramatically altered. Pedersen (1980) described four styles of mineralization in the Angel orebody: banded, massive, porphyroclastic, and coarse-grained, remobilized ore produced during the syntectonic deformation and metamorphism. The banded ore (Fig. 9a) is characterized by thin (mm to cm) layers of pyrite in sphalerite and galena bands. The contacts between the banded ore and the host marble are sharp and conformable, suggesting that these may reflect original contacts between the sulfides and the host carbonate. Intercalated, rotated clasts of marble in the banded ore are present and pyrite annealing was observed. Banded ore zones transition into zones of massive ore in areas associated with more intense shear deformation and ductile/brittle transformations (Fig. 8). The porphyroclastic ore zones (Fig. 9b) are associated with thrust sheets (Fig. 8) and occur as thin horizons of ductilly remobilized sphalerite and galena with brittle clasts of pyrite and marble (Pedersen 1980). The remobilized ore occurs in low-pressure zones in the folded ore bodies (Fig. 8) and consists mainly of sphalerite and galena associated with pinch and swell features (Pedersen 1980).

A paragenetic sequence presented by Horn et al. (2019) for the most intensely deformed ore assemblage (porphyroclastic ores of Pedersen 1980, 1981) was interpreted to represent a syn-deformation, high-temperature, hydrothermal event (see discussion below in Deposit classification). Horn et al. (2019) also described breccia ore (Fig. 10) that consists of a matrix of massive sulfides, supporting clasts of angular and folded marble fragments, which was interpreted as evidence for coeval mineral deposition with or post-dating regional deformation. However, these types of textures are common in sediment-hosted deposits that were deformed and metamorphosed (e.g., McDonald 1970; Clark and Kelly 1973; Jansson et al. 2018; Leach and Song 2019; Zhao et al 2021.

The Black Angel mine can no longer be accessed, therefore structural data were collected as part of this study near the South Lakes Glacier occurrence southeast of the Black Angel deposit. These data are used to provide insights into the structural evolution of the deposit since both areas belong to the Black Angel tectonic unit and presumably have a common shared evolution (Guarnieri and Baker 2022). Planar fabric, foliation, and cleavage of marbles and metapelitic rocks, together with fold axes

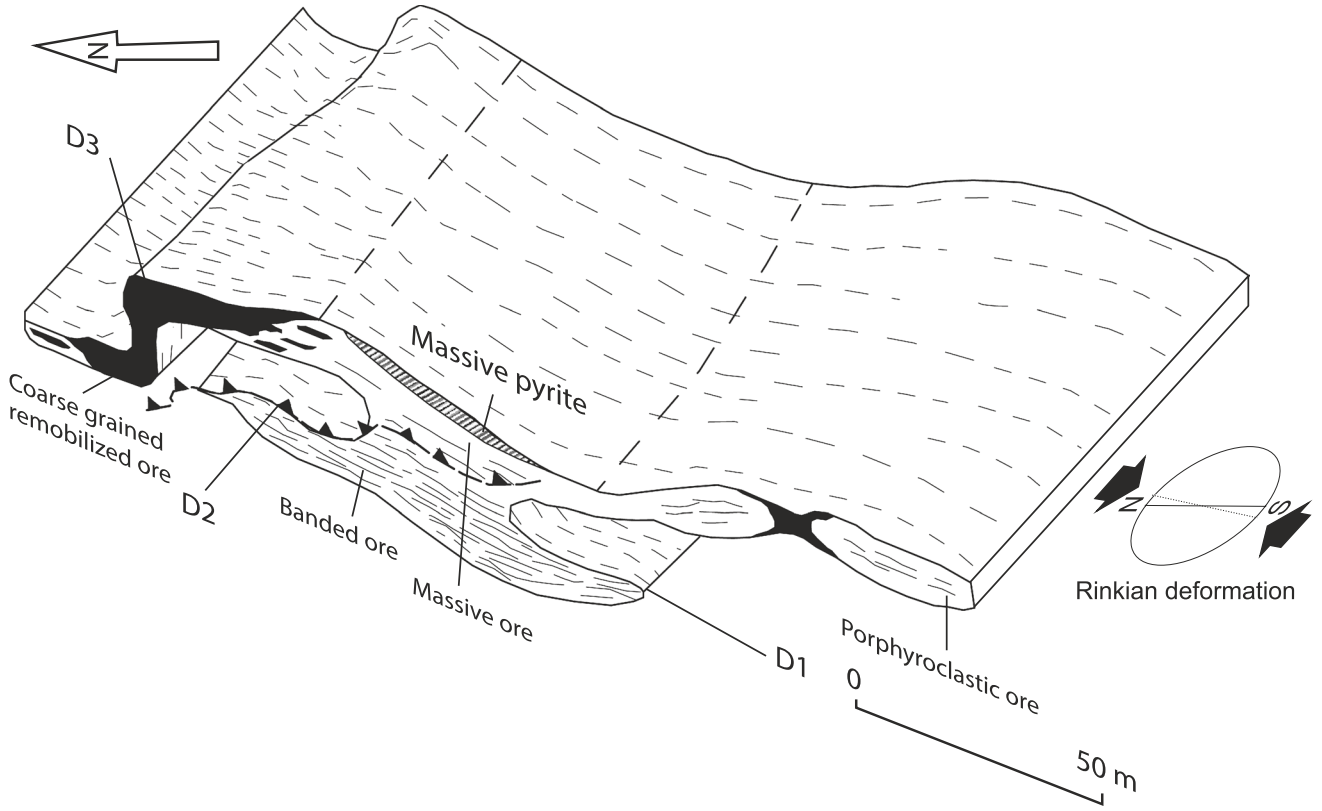

Fig. 8 Schematic representation of mesoscopic structures in the Angel orebody (modified from Pedersen 1980); see Fig. 2 for the location. D1-3 indicate, respectively, the early isoclinal folding, thrusting with southward directed displacement and late folding that are consistent with NNE-SSW-oriented compressional stress as indicated by black arrows

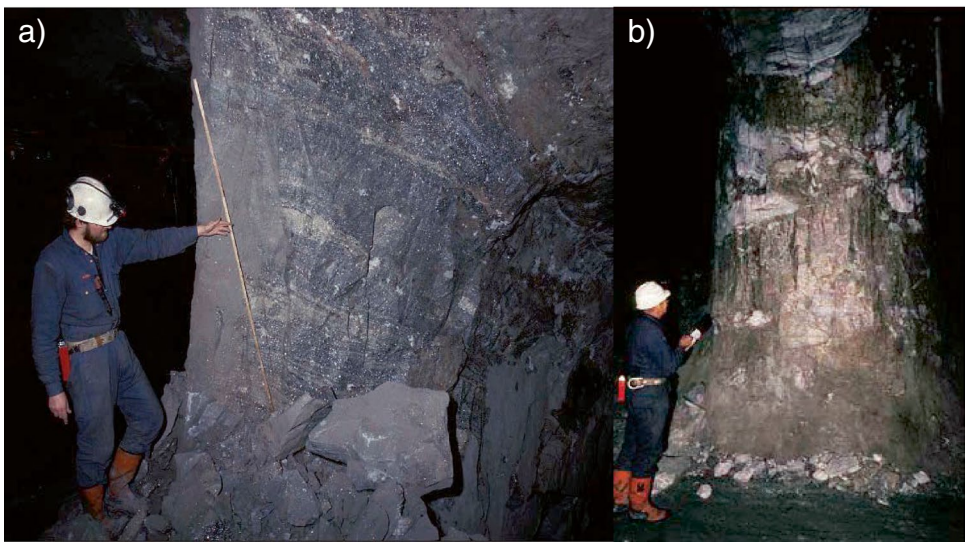

Fig. 9 Tectonic deformation of the Angel orebody showing ductile deformation of sphalerite and galena with clasts of marble: **a** rib pillar with high-grade banded ore; **b** porphyroclastic "buck shot" ore with marble rafts in the pillar. Photos are from Bjørn Thomassen (GEUS)

of small-scale folds and kinematic indicators along shear planes, are presented on stereoplots (Fig. 11) and the relationships among structures produced on different stages of deformation are discussed below.

Our observations document that the ore is present in extensional veins, along hinges of isoclinal folds in marbles of the Mârmorilik Formation (Fig. 11a). The WNW-ESE trend of fold axes is consistent with the Rinkian deformation

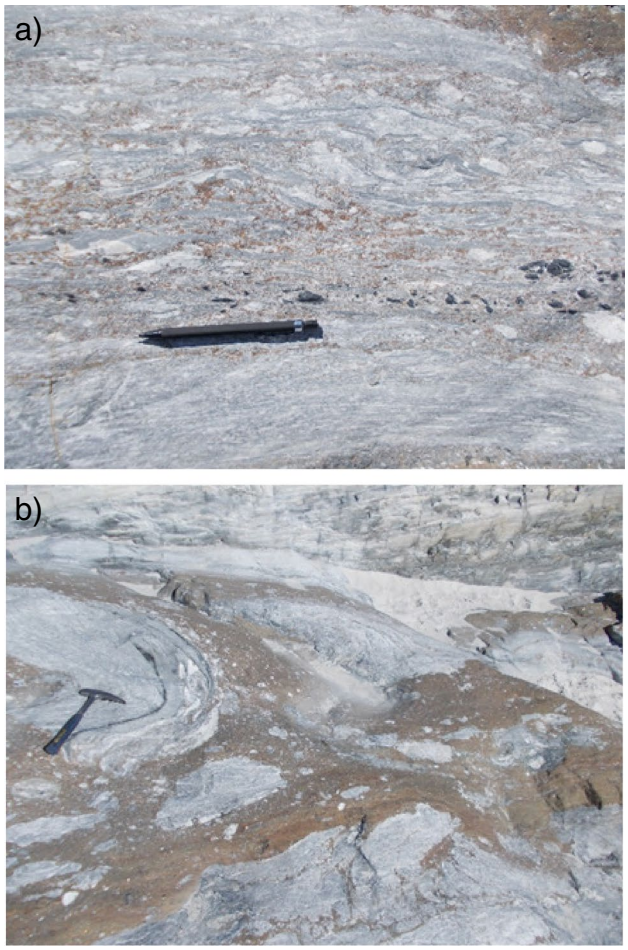

Fig. 10 Ore breccia in outcrop from the South Lakes Glacier occurrence: **a** the brown breccia matrix is ductilely remobilized sphalerite supporting clasts of silicified black pelite and marble; **b** larger marble clasts are sharp-edged and deformed. The interpretation is that the breccia-hosted ore was tectonically deformed, rather than being-formed coevally with brecciation, as previously inferred

(Guarnieri and Baker 2022) and the thick-skinned thrusting associated with the emplacement of a basement nappe (Henderson and Pulvertaft 1987). Folding and thrusting are associated with brittle faults and extensional veins (Fig. 11b, c), consistent with a maximum horizontal stress, oriented SSW-NNE (Fig. 11d). Planar fabric and fold hinges in the marbles are then overprinted by a second stage of brittle deformation with the development of upright folds and a pervasive NE-SW trending pressure solution cleavage with stylolites (Fig. 11e, f) that are interpreted as part of a NW–SE oriented compressional event possibly related to the latest stage of the Nagssugtoqidian Orogeny that formed NE-SW trending thrusts (Grocott and McCaffrey 2017; Guarnieri et al. 2022b).

The three deformation stages (D1-3, Fig. 8) introduced by Pedersen (1980) can be explained as the progression of a single tectonic event where thrusts, folds and extensional fractures are all consistent with NNE-SSW-oriented compression. The new data from ductile and brittle structures in the South Lakes area (Fig. 11) confirm this orientation of the tectonic stress, which can be correlated to the Rinkian Orogeny deformation, as constrained by regional mapping and structural studies (Grocott and McCaffrey, 2017; Guarnieri et al. 2022b; Guarnieri and Baker, 2022).

Discussion

Deposit classification

Pedersen (1980, 1981) documented the effects of greenschist facies metamorphism, intense multi-stage deformation and recrystallization on the ore deposits, finding that the original deposit morphologies, ore textures, geochemical zonation, and paragenetic relationships were modified or destroyed. Consequently, identifying the best genetic model requires a focus on the fundamental geological attributes of the deposit models proposed for the Black Angel deposit.

Models for the Black Angel deposit include sedimentary exhalative, Kipushi-style metamorphic-hydrothermal, and MVT mineralization. The classification as a sedimentary exhalative (SEDEX) type was based on the presence of stratabound and banded sulfides (Sangster 1990; Leach et al. 2005). Our observations indicate that the banded sulfide zones are due to the deformation. Moreover, sedimentary exhalative deposits do not form in a carbonate platform environment (Leach et al. 2010), hence this model is excluded. Horn et al. (2019) proposed that the deposit formed from a high-temperature hydrothermal fluid during shear deformation and metamorphism. Although these authors recognized the effects of intense deformation on the deposit, they interpreted the mineralization to be cogenetic with deformation and metamorphism. A Kipushi-type mineralization model (DeVos et al. 1974) was further proposed by Horn et al. (2019) based in part on the presence of trace mineral inclusions of Ge- and Sn-rich minerals (briartite and stannite, respectively) in sphalerite. An alternative interpretation to linking briartite and stannite in sphalerite with metamorphism and deformation is the recrystallization of preexisting sphalerite during metamorphism to create a new suite of trace minerals, including Ge-rich briartite inclusions in sphalerite (Frenzel et al. 2016; Cugerone et al. 2021).

In the absence of evidence for coeval magmatism and the depositional setting in a carbonate platform environment, a MVT-type model proposed by Carmichael (1988), Rosa et al. (2017), and Partin et al. (2021) is reasonable. MVT deposits are hosted in carbonate rocks and are commonly associated with organic matter. These latter factors also apply to some CD deposits although siliciclastic rocks characteristically dominate the rock sequence hosting the

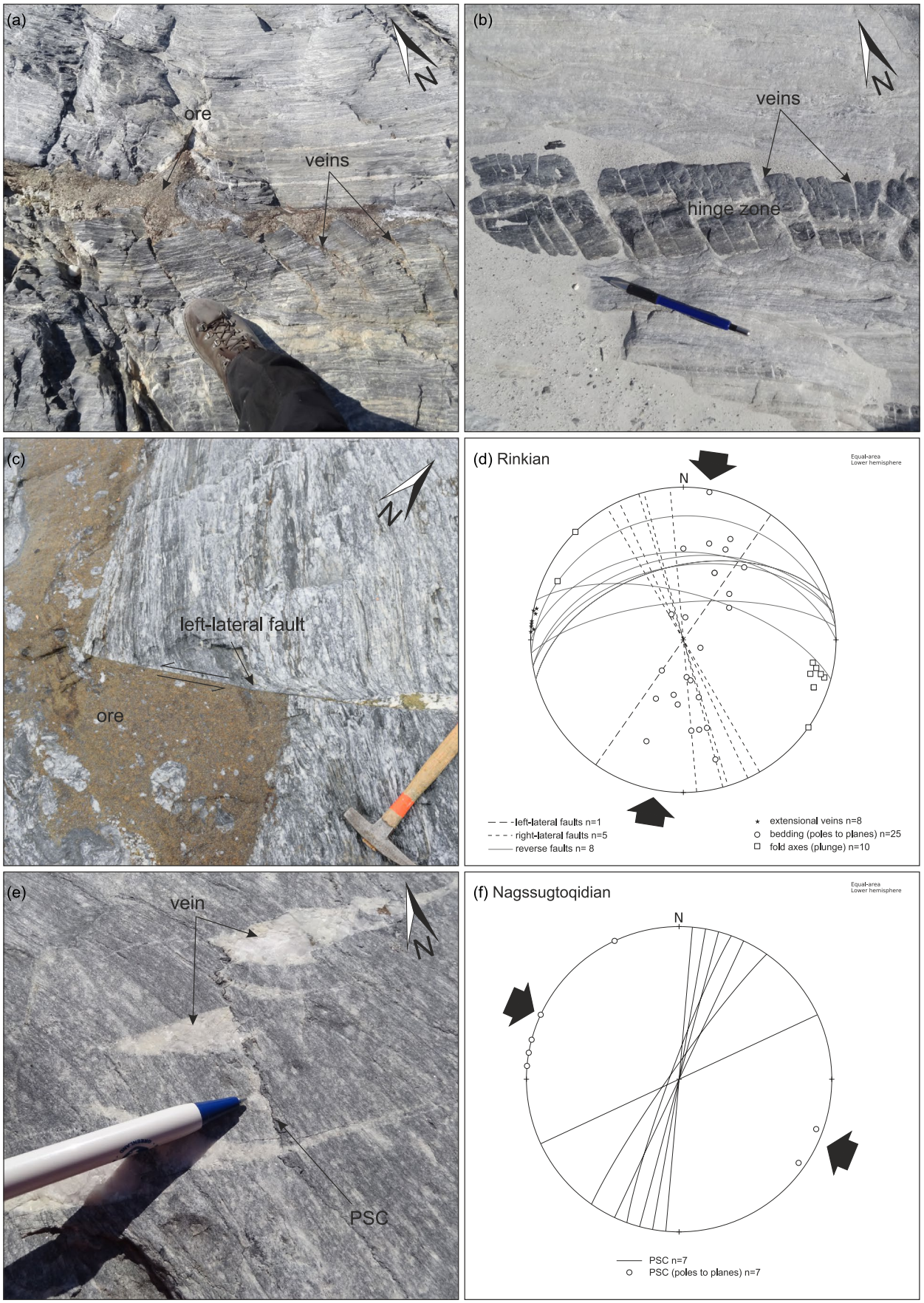
(a)
ore
veins
N
(b)
veins
hinge zone
N
(c)
left-lateral fault
ore
N
(d) Rinkian
Equal-area
Lower hemisphere
N
left-lateral faults n=1
right-lateral faults n=5
reverse faults n= 8
extensional veins n=8
bedding (poles to planes) n=25
fold axes (plunge) n=10
(e)
vein
PSC
N
(f) Nagssugtoqidian
Equal-area
Lower hemisphere
N
PSC n=7
PSC (poles to planes) n=7

◂**Fig. 11** Structural data from the South Lakes area (see Fig. 2 for location). Rinkian and Nagssugtoqidian orogenic deformation affected marbles of the Mârmorilik Formation and Black Angel deposit: **a** WNW-ESE-trending banded marbles crosscut by extensional veins filled with sulfides; **b** hinge zone of a WNW-ESE trending fold crosscut by NNE-SSW-trending calcite veins. The "domino-like" structure is likely related to bending of the fold axis during tectonic transport; **c** NE-SW-trending left-lateral fault crosscuts the planar fabric of marbles and the ore; **d** lower hemisphere stereoplot of mesoscale structures associated with pure-shear deformation that is consistent with the Rinkian NNE-SSW-oriented compression, responsible for the syntectonic recrystallization and ductile transport of sphalerite and galena during the D1-3 deformation (Fig. 8); **e** planar fabric of marbles and Rinkian extensional veins crosscut by subvertical pressure solution cleavage (PSC) with stylolites; **f** lower hemisphere stereoplot of PSC post-dating Rinkian structures and consistent with NW–SE-oriented Nagssugtoqidian orogenic compression

latter deposits (Leach et al. 2010). The generally accepted MVT models involve fluid mixing and fluid-rock interactions where oxidized metal-rich fluids mix with reduced sulfur that was locally produced by either bacterial sulfate reduction (BSR) or thermochemical sulfate reduction (TSR). Partin et al. (2021) determined the $\delta^{34}S$ composition of sulfide minerals (pyrite, sphalerite, galena, and pyrrhotite; 104 SIMS analyses on 4 samples) from the Black Angel deposit to be between 0‰ and + 6.9‰ and suggested that the reduced sulfur may have been produced by both BSR and TSR of low sulfate-bearing middle Paleoproterozoic seawater (Planavsky et al. 2012; Turner and Bekker 2016). Our sulfur isotope data are limited, but based on our anhydrite values, seawater sulfate was likely lower than the + 20‰ value assumed by Partin et al. (2021). However, the data are not robust enough to determine relative roles of BSR and TSR. Regardless, the reduced sulfur produced in the basin was subsequently trapped in a hydrocarbon/reduced sulfur trap or migrated into the ore zone through fault zones or along permeability boundaries in the host sequence (e.g., limestone to dolostone).

The role of evaporites in the Mârmorilik Formation carbonate platform

An important contribution of this study is the recognition of the close association of anhydrite and vanished evaporites within the Black Angel deposit and associated mineral occurrences that was underappreciated in previous publications. The connection between evaporites and sediment-hosted Zn–Pb deposits has been mainly limited to the well-established link between the origin of the ore-forming brines and dissolved evaporite sequences (Kesler et al. 1996; Viets et al. 1996; Leach et al. 2005, 2010 and references therein). Until recently, MVT deposits having a direct association with evaporites and former evaporite-bearing rocks were limited to a small subset of MVT deposits. Well-known examples are the deposits on the Lennard Shelf of the Canning basin, Australia (Tompkins et al. 1994; Vearncombe et al. 1995; Warren and Kempton 1997); Nanisivik, Canada (Ghazban et al. 1990); and Pine Point district, Canada (Sasaki and Krouse 1969). Three of the five largest MVT deposits in the world, Huoshaoyun, Jinding, and Changba-Lijiagou in China, are related to former evaporite-bearing sequences (Leach and Song 2019 and references therein). The Changba-Lijiagou deposits are hosted in meta-evaporites within an evaporite-carbonate platform of the Yangtze block in South China (Leach and Song 2019).

The deposition of evaporites and halokinetic processes do not create ores; rather, they should be viewed as providing ground preparation for later MVT mineralizing events. The ground preparation can be summarized as a product of two broad effects. One is that the presence of evaporites in a sedimentary sequence yields dramatic changes in porosity and permeability of the sedimentary rocks during diagenesis when secondary porosity, dissolution collapse breccias, halokinetic breccias, and structural and lithological traps are produced. Porosity and permeability impart significant control on the transfer of metalliferous fluids in sedimentary basins. The second effect is the development of chemical traps for metals carried by the MVT ore fluids (e.g., Jinding, China; Leach et al. 2017). Evaporite-bearing sequences containing gypsum and/or anhydrite provide an enormous reservoir of sulfur that can be reduced by BSR or TSR processes in the presence of organic matter, hydrocarbon, and reduced fluids. Some shales and carbonates are enriched in organic matter and, on burial, release hydrocarbons, whereas the most important lithological traps for hydrocarbons, reduced fluids, and sulfur are evaporites and massive limestones.

Cap rock for the Black Angel MVT deposit

An important characteristic of many MVT deposits is the presence of a cap rock or aquitard overlying the mineralization. These cap rocks are commonly shale, silicified dolostone (former evaporite-bearing dolostone), evaporites, or fine-grained limestone, which are interpreted to have served as a seal or stratigraphic barrier that focused hydrocarbon gas, reduced fluids, and/or reduced sulfur into a "chemical trap." The obvious cap rocks in the Mârmorilik Formation are the abundant semipelites (Fig. 2) that are spatially associated with the mineralization in the lower part of the Mârmorilik Formation or the massive calcitic marbles and thick graphitic semipelites that stratigraphically overlie the Black Angel deposit.

Possible analogs to the Black Angel deposit include the Florida Canyon and Shalipayco deposits in the Pucara basin, Peru (Oliveira et al. 2019, 2020, 2021), and the Mayuan and Maozu MVT deposits in China (Leach and Song 2019). These deposits have evaporites or vanished evaporites in the host sequence with significant mineralization in evaporite

dissolution breccia and related lithologies. Individual deposits are stratabound and extend laterally for kilometers, but have limited stratigraphic distribution (tens of meters). The Mayuan- and Maozu-style MVT occurrences and deposits occur over hundreds of kilometers in the Neoproterozoic (Sinian) carbonates of the Yangtze craton, South China (Leach and Song 2019). The ores are mainly hosted in evaporite dissolution collapse breccias, including float breccia. The Black Angel mine is inaccessible, and it is therefore impossible to fully evaluate the nature of the breccia-hosted mineralization. Considering that ore-hosting breccias in the Black Angel orebodies and associated showings (Fig. 10) occur in a former evaporitic carbonate sequence, we suggest the breccia may have been an evaporite dissolution float breccia that was subsequently deformed. Nevertheless, we cannot entirely exclude the possibility that the breccia originated as a carbonate dissolution breccia.

Timing of mineralization

The extensive evaporite-carbonate platform of the Mârmorilik Formation was likely a significant "brine factory" that charged the deep basin with highly saline fluids. Halite typically makes up more than 60–80% of the total rock salt volume in a marine basin (Warren 2016). Considering the abundance of anhydrite in the Mârmorilik Formation, an enormous volume of saline fluids must have been produced during the evaporation of seawater to form the evaporites. Following the well-established model for MVT deposits, the metalliferous brine migrates into the carbonate platform during major orogenic events or during basin inversion and deformation (e.g., Bradley and Leach 2003; Leach et al. 2005, 2010). The only published geochronological constraint for the Black Angel mineralization is an imprecise, Re-Os model age of 1570 ± 170 Ma (Partin et al. 2021), interpreted by the authors as "geologically meaningless" and therefore not considered herein. However, the age of the Mârmorilik Formation marble sequence is broadly constrained to be ca. 1915 Ma (see discussion in District Geology above). We infer that, subsequent to deposition of the Mârmorilik Formation, the Karrat basin became part of the foreland to both the Rinkian and Nagssugtoqidian orogens. As a result, brine that migrated during the Nagssugtoqidian Orogeny could have reached the Maarmorilik area. Albitization of Archean gneisses (Ryan and Escher 1999) and Paleoproterozoic metasedimentary rocks (Kalsbeek 1992), recognized in the Disko Bay area, approximately 100–150 km SSE of Uummannaq (Fig. 1), and located between the Maarmorilik area and the Nagssugtoqidian Orogen front, provides evidence for the extensive circulation of these brines. Based on the geochronology of the tectonic events (Fig. 12), mineralization took place after the Nagssugtoqidian collision at ca. 1860 Ma, but before the Rinkian orogenic metamorphism at ca. 1830 Ma. However, since the Nagssugtoqidian

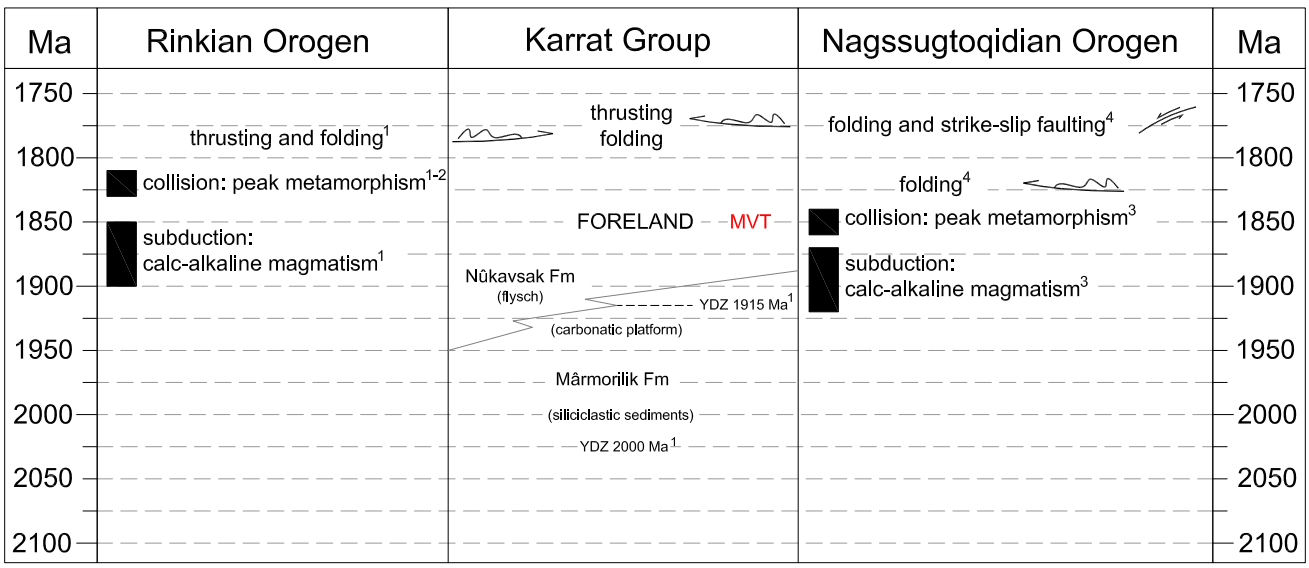

[1]Guarnieri et al. 2022b; [2]Kirkland et al. 2017; [3]Kalsbeek et al. 1987; [4]Connelly et al. 2000

Fig. 12 Summary of tectonic events related to the Rinkian and Nagssugtoqidian orogenies and their effects on the Mârmorilik Formation-mixed sulfate evaporite-carbonate platform. The platform became the foreland of the Nagssugtoqidian orogen at the beginning of the collisional stage at ca. 1860 Ma. As a result, migration of metal-bearing brines during the Nagssugtoqidian orogeny was to the north, towards the Mârmorilik Formation-mixed sulfate evaporite-carbonate platform and led to the formation of MVT deposits. The MVT deposits were developed before ca. 1830 Ma when they were affected by metamorphism and deformation associated with the Rinkian Orogeny. YDZ, youngest detrital zircon

Orogen was further away, the foreland was first affected by thin-skinned Rinkian deformation and later overprinted by thick-skinned thrusting developed at the Nagssugtoqidian orogenic front (Grocott and McCaffrey 2017; Guarnieri and Baker 2022).

Coupled evolution of Earth's hydrosphere and MVT deposits

The ore-forming brines for sediment-hosted MVT and CD deposits were derived from oxidized, marine evaporative environments along craton margins (e.g., Leach et al. 2010; Huston et al. 2016) that extracted metals from deep aquifers. The influx of these oxidized brines into reduced marine sediments produced CD deposits, whereas the brines that ascended into carbonate platforms during later orogenic events formed MVT deposits. The seawater sulfate concentration on the evolving Earth was a critical factor that controlled the distribution of sediment-hosted Zn–Pb deposits in the rock record (e.g., Holland 2005, 2006; Leach et al. 2005, 2010; Kesler and Reich 2006; Farquhar et al. 2010). At shallow crustal levels (typically having temperature < 250 °C), extraction of Zn and Pb from crustal materials and their transport are controlled by the redox state of sulfur in saline hydrothermal fluids in the hydrosphere and deep basins (e.g., Cooke et al. 2000). As a result, the distribution of MVT and CD deposits through Earth history (Leach et al. 2010 and references therein) is restricted to sedimentary successions younger than the Great Oxidation Episode (GOE) that started at ca. 2430 Ma (e.g., Bekker et al. 2004, 2020; Holland 2006, 2009; Poulton et al. 2021**).** This reflects a secular change in the redox conditions of the atmosphere and oceans that were major controls on the sulfate content of the ocean. Prior to the GOE, the reducing conditions in the atmosphere and oceans severely limited the mobility of Zn and Pb with saline, basinal fluids and therefore the formation of sediment-hosted Zn–Pb deposits. Notably, pseudomorphs of halite, but not sulfate, are recognized in a number of Archean sedimentary successions (e.g., Boulter and Glover 1986; Eriksson et al. 2005). This suggests that it is indeed low seawater sulfate content and lack of sulfate evaporites in the rock record, rather than lack or paucity of evaporite depositional settings and marine evaporites, which determined the general absence of MVT deposits in the Archean.

The ca. 1915 Ma age for the Mârmorilik Formation carbonate sequence places the Black Angel deposit as one of the few MVT or CD deposits hosted in Paleoproterozoic rocks, while only two are found in Archean rocks (Leach et al. 2005, 2010; Kesler and Reich 2006). Of the few deposits in Paleoproterozoic rocks, only the Black Angel deposit is clearly genetically linked to a hosting sulfate-rich, evaporite-carbonate sequence, although some of the others, described below, are hosted in or stratigraphically proximal to successions that record evaporative, marine conditions:

(a) The Pering and Bushy Park MVT deposits are hosted by the Neoarchean (2650 – 2520 Ma) Campbellrand Subgroup of the Transvaal Supergroup, South Africa. The mineralization age of 2100 to 2000 Ma (Duane et al. 2004; Schaefer et al. 2004) is temporally close to that of the hydrothermal circulation around the ca. 2060–2050 Ma Bushveld Igneous Complex, South Africa (Gleason et al. 2011), and younger than the GOE. There is no evidence for halite or sulfate-rich evaporites in the breccia or host sequence, but the overlying ca. 2200–2100 Ma Lucknow Formation of the Olifantshoek Group contains pseudomorphs after sulfate and halite evaporites (Schröder et al. 2008).
(b) The Esker MVT deposit and similar occurrences are hosted in the ca. 1890 Ma Rocknest Formation, northwestern Canadian Arctic (Gummer et al. 1997). Esker is a large and low-grade deposit containing sulfide matrix breccias (Kesler and Reich 2006). Gypsum pseudomorphs are reported locally in the hosting dolostone (Hoffman 1968, 1978; Badham and Stanworth 1977; Jackson 1989; Grotzinger 1986; Pope and Grotzinger 2003).
(c) The passive-margin CD deposits of the Zawar district, in the ca. 2000–1800 Ma Aravalli-Delhi orogen of India, are interpreted to have formed at about 1850 to 1800 Ma (Deb and Thorpe 2004; Sarkar and Banerjee 2004). Mineralization is commonly hosted in carbonate units within siliciclastic-dominated sequences. Disseminated anhydrite occurs in the underlying shales (Sarkar and Banerjee 2004).
(d) The ca. 1900 Ma Pb–Zn MVT deposit of the Paroo Station Mine on the Yilgarn craton of Western Australia is hosted by the Yelma Formation sulfate evaporite-carbonate-redbed succession (Pirajno and Burlow 2009; Sergeev et al. 2017).
(e) The MVT Zn–Pb deposits of the ca. 1900 Ma Ramah Group, Nain Province of northern Labrador in Canada have no known associations with evaporites (Wilton et al. 1994; Conliffe et al. 2013).
(f) The North Australia Zn belt contains several giant Zn–Pb–Ag CD deposits and the Mt Isa Cu ores are hosted in siliciclastic-dominated sedimentary sequences with minor occurrences hosted in carbonate units (possible MVT: Jones 1986; Plumb et al. 1980), developed in the ca. 1650–1600 Ma McNamara Group (Jones 1986; Andrews 1996; Page and Sweet 1998; Large et al. 2005; Leach et al. 2005). The correlative units, the Gunpowder Creek Formation, and Urquhart Shale, that host the Kamarga and Mt Isa Zn–Pb and Cu deposits, contain well-preserved pseudomorphs after sulfate

evaporites (McClay and Carlile 1978; Neudert and Russell 1981). The Coxco Zn–Pb deposit (possible MVT) in the McArthur basin is also hosted in the ca. 1650–1600 Ma McArthur Group in the North Australia Zn Belt (Walker et al. 1983). Mineralization occurs in dolostones above strata containing extensively developed gypsum pseudomorphs and cauliflower chert nodules (Walker et al. 1977; Muir 1987; Page and Sweet 1998; Page et al. 2000).

Sedimentary record of marine sulfate evaporites and MVT deposits in the Paleoproterozoic

During the early Paleoproterozoic, Earth's atmosphere–ocean system evolved from a mildly reduced to an oxygenated state during the GOE. Although the initial rise in atmospheric oxygen is reasonably well documented, the changes in the ocean redox state and related abundance of marine sulfate are less constrained. The oldest preserved shallow-marine, sulfate evaporites associated with carbonates and bearing stratiform Cu mineralization are in the 2420–2320 Ma Duitschland Formation of South Africa and the ca. 2320 Ma Gordon Lake Formation of the Huronian Supergroup of Canada (Martini 1979; Chandler 1988; Crockford et al. 2019). A significant increase in oxygenation of atmosphere and oceans subsequently occurred during the ca. 2220–2060 Ma Lomagundi Event (e.g., Bekker et al. 2006; Bekker and Holland 2012) that resulted in widespread deposition of marine sulfate evaporites. These are mostly indicated by pseudomorphs or molds of former anhydrite and gypsum in marginal marine sedimentary successions (Melezhik et al. 2005; Schröder et al. 2008; Bekker et al. 2006) with the exception of the Onega basin of the Fennoscandian Shield in Russia, which contains the locally developed lower evaporitic unit with carbonates, sulfates, halite, and bittern salts (Morozov et al 2010). The overlying Tulomozero Formation is a thick sequence of stromatolitic dolostones, magnesite, and red beds deposited at ca. 2090 Ma (Melezhik et al. 2005). These rocks were deposited in fluvial, playa, sabkha, and intertidal environments and contain syn-depositional anhydrite-bearing carbonate and chert pseudomorphs after gypsum. The evaporites occur over a thickness of 500 m within an area of more than 2000 km^2, indicating that a large marine sulfate reservoir developed by ca. 2090 Ma, although it is debated whether it was fully or partially open to the global ocean (e.g., Alfimova et al. 2022). The seawater sulfate reservoir is generally considered to collapse in the aftermath of the Lomagundi Event when redox state of the atmosphere–ocean decreased (cf. Planavsky et al. 2012; Bekker and Holland 2012; Scott et al. 2014), although the ca. 2020 Ma Kasegalik and McLeary formations of the Belcher Group on the Belchers Island, NWT, Canada, contain pseudomorphs of sulfate (Bell and Jackson 1974; Hodgskiss et al. 2019a, 2019b).

The ca. 1915 Ma age of the Mârmorilik Formation-mixed sulfate evaporite-carbonate platform is younger than the ages of the marine sulfate deposits described above. The Mârmorilik Formation-mixed sulfate-evaporite-carbonate platform potentially records the last known sulfate evaporite sequence (with thick stratigraphic intervals and beds of sulfate, rather than pseudomorphs of displacively grown sulfate crystals in sediments) until the Mesoproterozoic, ca. 1200 Ma Society Cliff Formation in the Baffin Island, Canada (Kah et al. 2001; Kah and Bartley 2011), and ca. 1250 Ma Grenville Series (Whelan et al. 1990). The Society Cliff Formation contains gypsum beds (1–250 cm thick) that constitute up to 15% of the exposed strata (Kah et al. 2001) and the amphibolite to granulite metamorphic facies Grenville Series contain anhydrite lenses up to 60 m thick, but typically lenses are only 1 to 15 m thick. The Society Cliff Formation also hosts the significant evaporite-related Nanisivik MVT deposit (Olson 1984; Ghazban et al. 1990), whereas the Grenville Series host the Balmat-Edwards-Pierrepont Zn–Pb deposits (Corriveau et al. 2007); the only two MVT districts developed in Mesoproterozoic rocks.

Intriguingly, the Mârmorilik Formation-mixed sulfate evaporite-carbonate platform is broadly correlative to other metasedimentary successions on the cratons of the northern part of Laurentia, which were not yet assembled together at that time, but also record evaporitic conditions: 1) the Lake Harbour Group of the Meta Incognita terrane in the southern part of Baffin Island (Hogarth and Griffin 1978; Belley and Groat 2020); (2) Wollaston Group of the Hearne craton, Saskatchewan (Chandler 1978; Tran et al. 2008); (3) Tavani Formation of the Upper Hurwitz Group, Hearne craton, NWT (Miller and Reading 1993; Davis et al. 2005); (4) Denault Formation of the Labrador Trough, Canada (Zentmyer et al. 2011); and (5) ca. 1890 Ma Rocknest Formation, Slave craton, northwestern Canadian Arctic (Hoffman 1968, 1978; Badham and Stanworth 1977; Pope and Grotzinger 2003). Furthermore, the giant copper deposit of the ca. 1900–1870 Ma Chiney Subgroup, Udakan Group, Aldan Shield (Siberia), is associated with red beds and evaporites (Bogdanov et al. 1966; Gablina 1990; Kovach et al. 2018). Paleomagnetic data position the Slave and Siberia cratons at ca. 1880 Ma close to each other at low latitudes (Buchan et al. 2016; Mitchell et al. 2010; Antonio et al. 2017), while other cratons are not paleomagnetically characterized for this time interval. However, based on tectonic reconstructions, the Hearne craton was close to the Superior craton and thus both were at the intermediate latitudes (Buchan et al. 2016). Importantly, all these successions record the transition from a passive continental margin to foreland basins during assembly of the Nuna-Columbia supercontinent (Pehrsson et al. 2016). This points to an important exploration criterion

in vectoring sediment-hosted base metal deposits, where evaporite-bearing successions deposited before orogenic events are the key. In summary, this compilation highlights that evaporitic conditions were widespread during this time interval on several cratons, suggesting an economic potential for undiscovered Cu–Pb–Zn sediment-hosted deposits in these and correlative supracrustal successions deposited on the low latitude-positioned cratons, which may have been overlooked to date.

Proterozoic seawater sulfate level and redox state and MVT deposits in the aftermath of the Lomagundi carbon isotope excursion

We cannot constrain seawater sulfate concentrations from our observations because a sequence of evaporite mineral precipitation (cf. Holland 1984) is not preserved by the Mârmorilik Formation. However, considering the extent of evaporitic conditions in Laurentia, Yilgarn, and Siberia, seawater sulfate concentration was likely above the Archean level, but below that during the Lomagundi Event. Interestingly, subsequent to extensive deposition of these marine sulfate evaporites, recording a substantial seawater sulfate reservoir, Granular Iron Formations (GIFs), was deposited at ca. 1880 Ma in several basins worldwide under shallow-marine conditions, indicating a major, transient, or long-sustained ocean deoxygenation at the time when Large Igneous Provinces (LIPs) were emplaced worldwide (Bekker et al. 2010, 2013). Chromium and iron isotope compositions of Proterozoic GIFs have been used to argue for low-oxygen levels in the atmosphere–ocean system (Planavsky et al. 2014; Wang et al. 2022), despite a striking contrast with the Cr isotope record of carbonates (Gilleaudeau et al. 2016). However, considering that some if not all Proterozoic GIFs correspond to ocean deoxygenation events (Bekker et al. 2010, 2013), these two sedimentary records could be reconciled with a view of a weakly oxygenated, mid-Proterozoic ocean episodically impacted by a strong flux of reductants in association with LIP emplacements.

Carbonate-hosted MVT deposits remained scarce in the rock record until the late Neoproterozoic and Cambrian when the number of deposits dramatically increased as the result of the Neoproterozoic Oxygenation Event (NOE), during which the oceans were further oxygenated (e.g., Fike et al. 2006; Sahoo et al. 2012; Williams et al. 2019). Oxidation state of the atmosphere and ocean finally reached modern levels in the early Paleozoic (Dahl et al. 2010; Lenton et al. 2016; Wallace et al. 2017; Lu et al. 2018; Krause et al. 2018). Consequently, Neoproterozoic and Phanerozoic MVT deposits and sulfate-bearing evaporites flourished. Leach et al. (2010) suggested that the nature of the carbonate platforms also limited the formation of MVT deposits during the Proterozoic. A dramatic increase in the relative abundance of carbonates with coarse, skeletal carbonate grains and fragments occurred in the late Neoproterozoic-Early Cambrian (Hazen et al. 2008 and references therein). This significantly increased carbonate platform permeability relative to the Proterozoic, fine-grained, stromatolitic, carbonate mudstones (Lucia 2007). As a result, Phanerozoic carbonate platforms have a greater potential, relative to Proterozoic platforms, for long-distance migration of sedimentary brines and the formation of MVT districts and deposits spread over hundreds of kilometers. In contrast, Proterozoic MVT deposits are typically single deposits or small groups of ore bodies hosted in breccia zone in evaporite-bearing dolostones and evaporite facies (Leach et al. 2005, 2010).

Sedimentary evaporites are highly susceptible to dissolution, halokinetic remobilization, and alteration, making it challenging to infer their secular distribution from rock records. In contrast, MVT and CD deposits that are genetically linked to evaporite environments in sedimentary successions are likely to survive even at high metamorphic grades in the rock record. Therefore, their secular distribution and that of their hosting rocks might bear a much less biased record of secular changes in deposition of sedimentary evaporites. The broad review of temporal distribution of the MVT and CD deposits presented above and previously discussed (e.g., Leach et al. 2005, 2010) agrees well with the general pattern of redox changes in the atmosphere–ocean system, highlighting a potential to constrain higher-resolution patterns with a more comprehensive temporal record of these deposits.

Summary

The Black Angel deposit is a significant non-magmatic Zn–Pb deposit hosted in marbles of the late Paleoproterozoic Mârmorilik Formation. The sub-horizontal, stratabound ore bodies are in anhydritic marbles and consist of massive to semi-massive sphalerite-galena-pyrite. The deposit was metamorphosed to greenschist facies conditions and extensively deformed and sheared.

An important contribution of this study is the recognition of the close association of anhydrite, meta-evaporites, and vanished and replaced evaporites with the Black Angel deposit and associated occurrences. There are no thick layered evaporites preserved in the Mârmorilik Formation, likely due to the greenschist metamorphism and deformation. However, anhydrite is present in the host marbles and ore zones as local patches and lenses. The most common occurrence of anhydrite is as disseminations in the host marbles, which can contain up to about 20% of anhydrite. The S isotopic composition of limited anhydrite samples from two ore zones in the Black Angel deposit ranges between 5.2 and 12.6‰ and likely reflects composition of

the contemporaneous marine sulfate reservoir. Scapolite is common in anhydritic marbles in the Black Angel deposit, the host marble sequence, and outcrops of dolomitic marbles, including the lower part of the Mârmorilik Formation. The scapolite has Cl- and Na-rich composition, consistent with the contribution of detrital feldspar and halite-gypsum mineral precursors. Considering the evidence for extensive scapolitization and limited evidence for sulfate evaporites in the sequence, this marine evaporite system produced significantly more halite than gypsum. The host marble sequence contains extensive zones of vuggy porosity, quartz nodules, and quartz "eyes" that reflect vanished evaporites. It seems that, despite the generally accepted low level of marine sulfate in the Paleoproterozoic in the aftermath of the GOE and the Lomagundi Event, an enormous volume of highly saline fluid was generated on the Mârmorilik-mixed sulfate evaporite-carbonate platform and likely descended into the deep basin. The ca. 1915 Ma Mârmorilik Formation carbonate sequence is the last known sulfate-rich evaporite sequence until the Mesoproterozoic (ca. 1250–1200 Ma) Society Cliff Formation in Baffin Island, Canada, and the Grenville Series in the Adirondack Lowlands in New York, USA.

Considering the most fundamental attributes of the mineralization and host sequence, a MVT model is a reasonable classification for the Black Angel deposit. The Mârmorilik Formation was a sulfate-rich, evaporative carbonate platform, a common setting for MVT deposits in the Phanerozoic. These deposits require a cap rock or seal to capture hydrocarbons or reduced sulfur that are then chemical traps for ascending ore fluids. The likely cap rocks in the Mârmorilik Formation were the abundant organic-rich semipelites that are spatially associated with mineralization in the lower part of the Mârmorilik Formation and the massive calcitic marbles that overlie the Black Angel deposits. The Black Angel mineralization was developed in the foreland of the Nagssugtoqidian Orogen with subsequent deformation related to the Nagssugtoqidian and Rinkian orogenies. The mineralization age can thereby be constrained to be between 1860 and 1830 Ma.

Recognizing that the Mârmorilik Formation-mixed sulfate evaporite-carbonate platform broadly correlates to other metasedimentary successions on the cratons of northern Laurentia that also record evaporitic conditions and some of which show MVT potential presents important exploration potential. The recognition of seawater evaporative factories, bearing sulfates, on these cratons should thus be taken as a first-order exploration criteria for CD and MVT deposits.

Supplementary Information The online version contains supplementary material available at https://doi.org/10.1007/s00126-022-01125-z.

Acknowledgements We gratefully acknowledge the support of GEUS colleagues, namely B. Thomassen for his insights and allowing us to use his photographs and A. Garde. We thank K. Pfaff of the Colorado School of Mines for the automated mineralogy analyses and C. Johnson and D. Adams of the US Geological Survey for providing the S isotope analysis and quantitative elemental analysis, respectively. We thank Y. Song, Institute of Geology, Chinese Academy of Geological Sciences, for valuable discussions. Finally, D. Huston and S. Pehrsson, as well as Associate Editor Karen Kelley, are acknowledged for their constructive reviews, which greatly helped to improve and clarify this manuscript.

Funding This work was carried out within the framework of the KarratZinc project, jointly financed by GEUS – Geological Survey of Denmark and Greenland and MMR – Ministry of Mineral Resources of Greenland. Participation by Andrey Bekker was supported by the ACS PF grant 624840ND2.

Declarations

Conflict of interest The authors declare no competing interests.

References

Alfimova NA, Kuznetsov AB, Klimova EV, Bekker A (2022) Archean-Proterozoic unconformity on the Fennoscandian Shield: geochemistry and Sr, C and O isotope composition of Paleoproterozoic carbonate-rich regolith from Segozero Lake (Russian Karelia). Precambrian Res 368:106459

Andrews S (1996) Stratigraphy and depositional setting of the upper McNamara Group, Lawn Hill region. James Cook University, Economic Geology Research Unit Contributions 55:5–9

Antonio PYY, D'Agrella MS, Trindade RIF, Nedelec A, de Oliveira DC, da Silva FF, Roverato M, Lana C (2017) Turmoil before the boring billion: Paleomagnetism of the 1880–1860 Ma Uatuma event in the Amazonian craton. Gondwana Res 49:106–129

Badham JPN, Stanworth CW (1977) Evaporites from Lower Proterozoic of East Arm. Great Slave Lake Nature 268(5620):516–518

Bekker A, Holland HD, Wang PL, Rumble D, Stein HJ, Hannah JL, Coetzee LL, Beukes NJ (2004) Dating the rise of atmospheric oxygen. Nature 427:117–120

Bekker A, Karhu JA, Kaufman AJ (2006) Carbon isotope record for the onset of the Lomagundi carbon isotope excursion in the Great Lakes area. North America Precambrian Res 148:145–180

Bekker A, Slack JF, Planavsky N, Krapež B, Hofmann A, Konhauser KO, Rouxel OJ (2010) Iron formation: the sedimentary product of a complex interplay among mantle, tectonic, oceanic, and biospheric processes. Econ Geol 105(3):467–508

Bekker A, Holland HD (2012) Oxygen overshoot and recovery during the early Paleoproterozoic. Earth Planet Sci Lett 317:295–304

Bekker A, Planavsky N, Krapež B, Rasmussen B, Hofmann A, Slack JF, Rouxel OJ, Konhauser KO (2013) Iron formations: their

origins and implications for ancient seawater chemistry, Treatise of Geochemistry. Elsevier, 561–628.
Bekker A, Krapež B, Karhu JA (2020) Correlation of the stratigraphic cover of the Pilbara and Kaapvaal cratons recording the lead up to Paleoproterozoic Icehouse and the GOE. Earth-Science Reviews, 211
Bell RT, Jackson GD (1974) Aphebian halite and sulphate indications in the Belcher Group, Northwest Territories. Can J Earth Sci 11:722–728
Belley PM, Groat LA (2020) Metamorphosed carbonate platforms and controls on the genesis of sapphire, gem spinel, and lapis lazuli: insight from the Lake Harbour Group, Nunavut, Canada and implications for gem exploration. Ore Geol Rev 116:103259
Bogdanov YV, Kochin GG, Kutyrev YI, Paradeeva LM, Travin LV, Trifonov NP, Feoktistov VP (1966) Medistye otlozheniya Olekmo-Vitimskoi gornoi strany (cupriferous deposits of the Olekma-Vitim Highland). Nedra, Leningrad, USSR, p 386
Bolhar R, Hofmann A, Woodhead J, Hergt J, Dirks P (2002) Pb- and Nd-isotope systematics of stromatolitic limestones from the 2.7 Ga Ngezi Group of the Belingwe Greenstone Belt: constraints on timing of deposition and provenance. Precambrian Res 114:277–294
Boulter CA, Glover JE (1986) Chert with relict hopper molds from Rocklea Dome, Pilbara Craton, Western Australia - an Archean Halite-Bearing Evaporite. Geology 14(2):128–131
Bradley DC, Leach DL (2003) Tectonic controls of Mississippi Valley-type lead-zinc mineralization in orogenic forelands. Miner Deposita 38:652–667
Buchan KL, Mitchell RN, Bleeker W, Hamilton MA, LeCheminant AN (2016) Paleomagnetism of ca. 2.13-2.11 Ga Indin and ca. 1.885 Ga Ghost dyke swarms of the Slave craton: implications for the Slave craton APW path and relative drift of Slave, Superior and Siberian cratons in the Paleoproterozoic. Precambr Res 275:151–175
Carmichael AJ (1988) the tectonics and mineralization of the Black Angel Pb-Zn deposits, central West Greenland. Unpublished thesis, Goldsmith's College, University of London, 371 p.
Chandler FW (1978) Geology of part of the Wollaston Lake Fold Belt, North Wollaston Lake, Saskatchewan. Geol Survey of Canada Bull 277:25
Chandler FW (1988) Diagenesis of sabkha-related, sulphate nodules in the Early Proterozoic Gordon Lake Formation, Ontario, Canada. Carbonates and Evaporites 3(1):75–94
Chown TM, Elkins JE (1974) The origin of quartz geodes and cauliflower cherts through the silicification of anhydrite nodules. J Sediment Petrol 44:885–903
Clark BR, Kelly WC (1973) Sulfide deformation studies: I. Experimental deformation of pyrrhotite and sphalerite to 2,000 bars and 500C:Econ. Geol 68:332–352
Conliffe J, Wilton DHC, Blamey NJF, Archibald SM (2013) Paleoproterozoic Mississippi Valley type Pb–Zn mineralization in the Ramah Group, Northern Labrador: Stable isotope, fluid inclusion and quantitative fluid inclusion gas analyses. Chem Geol 362:211–223
Connelly JN, van Gool JAM, Mengel FC (2000) Temporal evolution of a deeply eroded orogen: the Nagssugtoqidian Orogen. West Greenland Can J Earth Sci 37:1121–1142
Cooke D, Bull S, Large R, McGoldrick P (2000) The importance of oxidized brines for the formation of Australian Proterozoic stratiform sediment-hosted Pb-Zn deposits. Econ Geol 95:1–18
Corriveau L, Perreault S, Davidson A (2007) Prospective metallogenic settings of the Grenville Province. In: Mineral Deposits of Canada: A Synthesis of Major Deposit types, District Metallogeny, the Evolution of Geological Provinces, and Exploration Methods, Goodfellow WD (ed.). Geological Association of Canada, Special Publication 5: 819–48
Crockford PW, Kunzmann M, Bekker A, Hayles J, Bao HM, Halverson GP, Peng YB, Bui TH, Cox GM, Gibson TM, Worndle S, Rainbird R, Lepland A, Swanson-Hysell NL, Master S, Sreenivas B, Kuznetsov A, Krupenik V, Wing BA (2019) Claypool continued: extending the isotopic record of sedimentary sulfate. Chem Geol 513:200–225
Cugerone A, Cenki-Tok B, Muñoz M, Kouzmanov K, Oliot E, Motto-Rosa V, Goff Le (2021) Behavior of critical metals in metamorphosed Pb-Zn ore deposits:example from the Pyrenean Axial Zone. Miner Deposita 56:685–705
Dahl TW, Hammarlund EU, Anbar AD, Bond DPG, Gill BC, Gordon GW, Knoll AH, Nielsen AT, Schovsbo NH, Canfield DE (2010) Devonian rise in atmospheric oxygen correlated to the radiations of terrestrial plants and large predatory fish. Proc Natl Acad Sci USA 107(42):17911–17915
Davis WJ, Rainbird RH, Aspler LB, Chiarenzelli JR (2005) Detrital zircon geochronology of the Paleoproterozoic Hurwitz and Kiyuk groups, western Churchill Province, Nunavut. Geological Survey of Canada Current Research, 2005-F1: 13
Deb M, Thorpe RI (2004) Geochronological constraints in the Precambrian geology of Rajasthan and their metallogenic implications. In: Deb M, Goodfellow WD (eds) Sediment-hosted lead-zinc sulphide deposits: New Delhi. Narosa Publishing House, India, pp 246–263
Dejonghe L, Demaiffe D, Weis D (1998) Strontium isotope geochemistry of anhydrites and calcite pseudomorphs after anhydrite from Palaeozoic formations in Belgium. Chem Geol 144(1–2):63–71
DeVos W, Viaene W, Moreau J, Wautier J (1974) Mineralogie du gisement de Kipushi, Shaba, Zaire, in: Bartholom P, ed., Gisement stratiformes province cupriferes Liege, Soc. Geol. Belgique: 165–183
Duane MJ, Kruger FJ, Turner AM, Whitelaw HT, Coetzee H, Verhagen B (2004) The timing and isotopic character of regional hydrothermal alteration and associated epigenetic mineralization in the western sector of the Kaapvaal craton (South Africa). J Afr Earth Sc 38:461–476
Eriksson KA, Simpson EL, Master S, Henry G (2005) Neoarchaean (c. 2.58 Ga) halite casts: implications for palaeoceanic chemistry. Jour Geol Soc London 162:789–799
Fareeduddin VBR, Hanumantha R, Golani PR, Sharma BB, Neogi N (2014) Petrology and stable isotope (S, C, O) studies of selected sediment-hosted basemetal ore deposits in the Proterozoic Aravalli-Delhi Fold Belt, Rajasthan. Journal Geological Society of India 83:119–141
Farquhar J, Namping W, Canfield DE, Oduro H (2010) Connections between sulfur cycle evolution, sulfur isotopes, sediments, and base metal sulfide deposits. Econ Geol 105:509–533
Fike DA, Grotzinger JP, Pratt LM, Summons RE (2006) Oxidation of the Ediacaran Ocean. Nature 444:744–747
Frenzel M, Hirsch T, Gutzmer J (2016) Gallium, germanium, indium, and other trace and minor elements in sphalerite as a function of deposit type — a meta-analysis. Ore Geol Rev 76:52–78
Gablina IF (1990) Mineralogical-Geochemical Criteria for the Recognition of Red Rock Associations in Precambrian Metamorphic Sequences in Connection with Their Copper Potential. Lithology and Mineral Deposits 25(3):95–109
Garde A, Pulvertaft TCR (1976) Age relations of the Precambrian Mârmorilik Marble Formation, Central West Greenland: Rapp. Grønlands Geol Unders 80:49–53
Garde A (1978) The Lower Marmorilik Formation, East of Mârmorilik, West Greenland, Meddellerler om Grønland, 200, 3, 71 p + 6 plates
Gavelin S, Parwel A, Ryhage R (1960) Sulfur isotope fractionation in sulfide mineralization. Econ Geol 55:510–530
Ghazban F, Schwarcz HP, Ford DC (1990) Carbon and sulfur isotope evidence for in situ reduction of sulfate, Nanisivik lead-zinc

deposits, Northwest Territories, Baffin Island. Canada Econ Geol 85:360–375
Gilleaudeau GJ, Frei R, Kaufman AJ, Kah LC, Azmy K, Bartley JK, Chernyavskiy P, Knoll AH (2016) Oxygenation of the mid-Proterozoic atmosphere: clues from chromium isotopes in carbonates. Geochemical Perspectives Letters 2(2):178–187
Gleason JD, Gutzmer J, Kesler SE, Zwingmann H (2011) 2.05-Ga isotopic ages for Transvaal Mississippi Valley-Type deposits: evidence for large-scale hydrothermal circulation around the bushveld igneous complex. South Africa J Geol 119:69–80
Gomez-Pugnaire MT, Franz G, Lopez V, Sanchez-Vizcaino VL (1994) Retrograde formation of NaCl-scapolite in high pressure metaevaporites from the Cordilleras Beticas (Spain). Contr Mineral and Petrol 116:448–461
Grocott J, McCaffrey K (2017) Basin evolution and destruction in an Early Proterozoic continental margin: the Rinkian fold–thrust belt of central West Greenland. J Geol Soc 174(3):453–467
Grotzinger JP (1986) Cyclicity and paleoenvironmental dynamics, Rocknest platform, northwest Canada. Geol Soc Am Bull 97:1208–1231
Guarnieri P, Partin C, Rosa D (2016). Palaeovalleys at the basal unconformity of the Palaeoproterozoic Karrat Group, West Greenland. Geological Survey of Denmark and Greenland Bulletin, 35. https://doi.org/10.34194/geusb.v35.4940
Guarnieri P, Baker N, Rosa D, Sørensen EV (2022a) Geological map of Greenland 1:100 000, Nuugaatsiaq 71 V.2 Nord. Geological Survey of Denmark and Greenland, Copenhagen
Guarnieri P, Baker N, Rosa D, Sørensen EV (2022b) Geological map of Greenland 1:100 000, Maarmorilik 71 V.2 Syd. Geological Survey of Denmark and Greenland, Copenhagen
Guarnieri P, Rosa D, Thrane, K, Kokfelt, TF, Sørensen EV. Baker N (2022c) Paleoproterozoic Cordilleran-Type Tectonics in central West Greenland. EGU22–13531, Vienna EGU General Assembly
Guarnieri P, Baker N, Rosa D, Sørensen EV (2022d) Geological map of Greenland 1:100 000, Pannertooq 72 V.2 Syd. Geological Survey of Denmark and Greenland, Copenhagen
Guarnieri P, Thiele S, Baker N, Sørensen EV, Kirsch M, Lorenz S, Rosa D, Unger G, Zimmermann R (2022e) Unravelling the deformation of Paleoproterozoic marbles and Zn-Pb ore deposits, combining 3D-photogeology and hyperspectral data (Black Angel mine, central West Greenland). Submitted to Minerals
Guarnieri P, Baker, N (2022) Tectonic inversion of listric normal faults in the foreland of the Rinkian orogen (Maarmorilik, central West Greenland). J Struct Geol 159:104598
Gummer PK, Plint HE, Rainbird RH (1997) The Esker Lake prospect: Stratabound Pb-Zn-Cu-Ag in emergent inner shelf carbonates, Rocknest Formation, Coronation Supergroup, NWT: Yellowknife, NWT Geological Mapping Division, Exploration Overview, v. 1996, 3.18–3.19
Hanor JS (2004) A model for the origin of large carbonate- and evaporite-hosted celestine (SrSO4) deposits. J Sediment Res 74(2):168–175
Harris CJ (1985) Greenex A/S. South Lakes - Plateau drilling, Maarmorilik - West Greenland. 1984 year end report. Period covered: May - August 1984. Internal report, Greenex A/S, 23 pp., 11 plates, 12 photos. [13 drill logs]. https://data.geus.dk/gg_detail/?cat=rap&id=25637. Accessed May 2022
Harris CJ (1986) Greenex 1985. Black Angel surface drilling. Year end report. Internal report, Greenex A/S, 19 pp., [drill logs], 4 photos. 6 appendices. https://data.geus.dk/gg_detail/?cat=rap&id=25636. Accessed May 2022
Hazen RM, Papineau D, Bleeker W, Downs RT, Ferry JM, McCoy TJ, Sverjensky DA, Yang H (2008) Mineral evolution. Am Minerol 93:1693–1720
Henderson G, Pulvertaft TCR (1967) The stratigraphy and structure of the Precambrian rocks of the Umanak area, West Greenland. Medd Fra Dansk Geol Forening København 17:22
Henderson G, Pulvertaft TCR (1987) Descriptive text to geological map of Greenland 1 : 100 000, Mârmorilik 71 V.2 Syd, Nûgâtsiaq 71 V.2 Nord and Pangnertôq 72 V.2 Syd. Geological Survey of Greenland (GGU), Copenhagen, Denmark, 72
Hodgskiss MSW, Dagnaud OMJ, Frost JL, Halverson GP, Schmitz MD, Swanson-Hysell NL, Sperling EA (2019a) New insights on the Orosirian carbon cycle, early Cyanobacteria, and the assembly of Laurentia from the Paleoproterozoic Belcher Group. Earth Planet Sci Lett 520:141–152
Hodgskiss MSW, Crockford PW, Peng YB, Wing BA, Horner TJ (2019b) A productivity collapse to end Earth's Great Oxidation. Proc Natl Acad Sci USA 116(35):17207–17212
Hoffman PF (1968) Stratigraphy of the Lower Proterozoic (Aphebian), Great Slave Supergroup, East Arm of Great Slave Lake, District of Mackenzie. Geological Survey of Canada Paper 68–42. Dept. of Energy, Ottawa, 93
Hoffman PF (1978) Speleothems and Evaporite Solution Collapse in Athapuscow Aulacogen (Middle Precambrian), Great Slave Lake, Northwest Territories. AAPG Bull Am Assoc Pet Geol 62(3):523–523
Hogarth DD, Griffin WL (1978) Lapis Lazuli from Baffin Island - Precambrian meta-evaporite. Lithos 11(1):37–60
Holland HD (1984) The chemical evolution of the atmosphere and ocean. Princeton Series in Geochemistry. Princeton University Press, Princeton, NJ: 582
Holland HD (2005) Sedimentary mineral deposits and the evolution of Earth's near-surface environments. Econ Geol 100:1489–1509
Holland HD (2006) Oxygenation of the atmosphere and oceans. Philos Trans R Soc B 361:903–915
Holland HD (2009) Why the atmosphere became oxygenated: a proposal. Geochim Cosmochim Acta 73:5241–5255
Horn S, Dziggel A, Kolb J, Sindern S (2019) Textural characteristics and trace element distribution in carbonate-hosted Zn-Pb-Ag ores at the Paleoproterozoic Black Angel deposit, central West Greenland. Mineral Deposita 54:507–524
Hudec MR, Jackson MPA (2006) Growth of allochthonous salt sheets in passive margins and orogens. AAPG Bull 90:1535–1564
Hudec MR, Jackson MPA (2007) Terra infirma: Understanding salt tectonics. Earth Science Review 82:1–28
Huebner JS, Woodruff ME (1985) Chemical compositions and critical evaluation of microprobe standards available in the Reston microprobe facility: USGS Open-File Report 85–718, p 234
Huston DL, Champion D, Mernagha P, Downes M, Jones P, Forster D, Vladimir D (2016) Metallogenesis and geodynamics of the Lachlan Orogen: new (and old) insights from spatial and temporal variations in lead isotopes. Ore Geol Rev 76:257–267
Jackson M (1989) Early Proterozoic Cowles Lake foredeep reef, NWT, Canada. In: Geldsetzer, H.H.J., James, N.P., Tebbutt, G.E. (Eds.), Reefs, Canada and Adjacent Area. Canadian Society of Petroleum Geologists, Memoir 13, Calgary, Alberta, Canada, 64–71
Jansson NF, Sadbom S, Allen RL, Billstom K, Spry PG (2018) The Lovisa stratiform Zn-Pb deposit, Bergslagen, Sweden: structure, stratigraphy, and ore genesis. Econ Geol 113:699–739
Johnson CA, Stricker CA, Gulbransen CA, Emmons, MP (2018) Determination of $\delta^{13}C$, $\delta^{15}N$, or $\delta^{34}S$ by isotope-ratio-monitoring mass spectrometry using an elemental analyzer: U.S. Geological Survey Techniques and Methods, book 5, chp. D4: 19
Jones DA (1986) The Kamarga deposit: Stratabound zinc-lead mineralization in the middle Proterozoic McNamara Group, Northwest Queensland: Unpublished Ph.D. thesis, Armidale, New South Wales, Australia, University of New England, 209
Kah LC, Lyons TW, Chesley JT (2001) Geochemistry of a 1.2 Ga carbonate-evaporite succession, northern Baffin and Bylot Islands;

implications for Mesoproterozoic marine evolution. Precambr Res 111:203–234
Kah LC, Bartley JK (2011) Protracted oxygenation of the Proterozoic. Int Geol Rev 53:1424–1442
Kah LC, Lyons TW, Frank TD (2004) Low marine sulphate and protracted oxygenation of the Proterozoic biosphere. Nature 431:834–838
Kalsbeek F (1992) Large-scale albitisation of siltstones on Qeqertakavsak island, northeast Disko Bugt, West Greenland. Chem Geol 95:213–233
Kalsbeek F, Pidgeon RT, Taylor PN (1987) Nagssugtoqidian mobile belt of West Greenland: a cryptic 1850 Ma suture between two Archaean continents–chemical and isotopic evidence. Earth Planet Sci Lett 85:365–385
Kalsbeek F, Pulvertaft TCR, Nutman AP (1998) Geochemistry, age and origin of metagreywackes from the Palaeoproterozoic Karrat Group, Rinkian Belt, West Greenland. Precambr Res 91:383–399
Kesler SE, Reich MH (2006) Precambrian Mississippi Valley-type deposits: relation to changes in composition of the hydrosphere and atmosphere. Geol Soc Am Mem 198:185–204
Kesler SE, Martini AM, Appold MS, Walter LM, Huston TJ, Furman FC (1996) Na–Cl–Br systematic of fluid inclusions from Mississippi Valley-type deposits, Appalachian basin: constraints on solute origin and migration paths. Geochim Cosmochim Acta 60:225–233
King AR (1983) Greenex A/S. Report on prospecting and correlation programme in the Maarmorilik Formation, West Greenland 1982. Internal report, Greenex A/S, 21 pp., 12 plates. https://data.geus.dk/gg_detail/?cat=rap&id=24547. Accessed May 2022
Kirkland CL, Hollis J, Danišík M, Petersen J, Evans NJ, McDonald BJ (2017) Apatite and titanite from the Karrat Group, Greenland; implications for charting the thermal evolution of crust from the U-Pb geochronology of common Pb bearing phases. Precambr Res 300:107–120
Kolb J, Keiding J, Steenfelt A, Secher K, Keulen N, Rosa D, Stensgaard BM (2016) Metallogeny of Greenland. Ore Geol Rev 78:493–555
Kovach VP, Kotov AB, Gladkochub DP, Tolmacheva EV, Velikoslavinsky SD, Gorokhovsky BM, Podkovyrov VN, Zagornaya NY, Plotkina YV (2018) Age and Sources of Metasandstone of the Chiney Subgroup (Udokan Group, Aldan Shield): results of U-Th-Pb Geochronological (LA-ICP-MS) and Nd Isotope Study. Dokl Earth Sci 482(1):1138–1141
Krause AJ, Mills BJW, Zhang S, Planavsky NJ, Lenton TM, Poulton SW (2018) Stepwise oxygenation of the Paleozoic atmosphere. Nat Commun 9:4081
Large RR, Bull SW, McGoldrick PJ, Derrick, G, Carr, Walters GS (2005), Stratiform and strata-bound Zn-Pb-Ag deposits of the Proterozoic sedimentary basins of northern Australia. In: Hedenquist JW, Thompson JFH, Goldfarb RJ, Richards JP (eds) Econ Geol 100th Anniversary Volume, pp 931−963
Leach DL, Sangster DF, Kelley KD, Large RR, Garven G, Allen CR, Gutzmer J, Walters S (2005) Sediment-hosted lead–zinc deposits: a global perspective. In: Hedenquist JW, Thompson JFH, Goldfarb RJ, Richards JP (eds) Econ Geol 100th Anniversary Volume, pp 561–607
Leach DL, Bradley D, Huston D, Pisarevsky SA, Taylor RD, Gardoll SJ (2010) Sediment-hosted lead-zinc deposits in Earth History. Econ Geol 105:593–625
Leach DL, Song YC, Hou ZQ (2017) The world-class Jinding Zn–Pb deposit: ore formation in an evaporite dome, Lanping Basin, Yunnan, China. Miner Deposita 52:281–296
Leach DL, Song YC (2019) Sediment-hosted zinc-lead and copper deposits in China. In: Chang Z, Goldfarb R (eds) Mineral Deposits of China, Society of Economic Geologists, Inc., Special Publication 22: 325–409
Lenton TM, Dahl TW, Daines SJ, Mills BJW, Ozaki K, Saltzman MR, Porada P (2016) Earliest land plants created modern levels of atmospheric oxygen. Proc Natl Acad Sci USA 113(35):9704–9709
Lu WY, Ridgwell A, Thomas E, Hardisty DS, Luo G, Algeo TJ, Saltzman MR, Gill BC, Shen YN, Ling HF, Edwards CT, Whalen MT, Zhou XL, Gutchess KM, Jin L, Rickaby REM, Jenkyns HC, Lyons TW, Lenton TM, Kump LR, Lu ZL (2018) Late inception of a resiliently oxygenated upper ocean. Science 361(6398):174–177
Lucia, F.J., 2007, Carbonate reservoir characterization—an integrated approach, 2nd ed.: Berlin, New York, Springer, 336 p
Martini JEJ (1979) A copper-bearing bed in the Pretoria Group in northeastern Transvaal, Geokongress '77. Geological Society of South Africa Special Publication 6:65–72
McClay KR, Carlile DG (1978) Mid-Proterozoic sulphate evaporites at Mount Isa mine, Queensland, Australia. Nature 274:240–241
McDonald JA (1970) Some effects of deformation on sulfide-rich layers in lead-zinc ore bodies, Mount Isa. Queensland Econ Geol 65:273–298
Mckibben MA, Williams AE, Okubo S (1988) Metamorphosed Plio-Pleistocene evaporites and the origins of hypersaline brines in the Salton-Sea Geothermal System, California - Fluid Inclusion Evidence. Geochim Cosmochim Acta 52(5):1047–1056
Melezhik VA, Fallick AE, Rychanchik DV, Kuznetsov AB (2005) Palaeoproterozoic evaporites in Fennoscandia: implications for seawater sulphate, the rise of atmospheric oxygen and local amplification of the δ13C excursion. Terra Nova 17:141–148
Miller AR, Reading KL (1993) Iron-formation, evaporite, and possible metallogenetic implications for the Lower Proterozoic Hurwitz Group, District of Keewatin, Northwest Territories. Current Research, Part C; Geological Survey of Canada, Paper 93–1C: 179–185
Mitchell RN, Hoffman PF, Evans DAD (2010) Coronation loop resurrected: oscillatory apparent polar wander of Orosirian (2.05–1.8 Ga) paleomagnetic poles from Slave craton. Precambrian Research 179(1–4):121–134
Moine B, Sauvan P, Jarousse J (1981) Geochemistry of evaporite-bearing series: a tentative guide for the identification of metaevaporites. Contrib Mineral Petrol 76:401–412
Mora CI, Valley JW (1989) Halogen-rich scapolite and biotite; implications for metamorphic fluid-rock interaction. Am Miner 74(7–8):721–773
Morozov AF, Khakhaev BN, Petrov OV, Gorbachev VI, Tarkhanov GV, Tsvetkov LD, Erinchek YM, Akhmedov AM, Krupenik VA, Sveshnikova KY (2010) Rock salt mass in the Paleoproterozoic sequence of the Onega Trough in Karelia (from the Onega Parametric Well Data). Dokl Akad Nauk SSSR 435(1):1483–1486
Muir MD (1987) Facies models for Australian precambrian evaporites. In: Evaporite Basins, Pery TM (ed). Lecture Notes in Earth Sciences, 13. Springer, Berlin, Heidelberg
Neudert MK, Russell RE (1981) Shallow-Water and Hypersaline Features from the Middle Proterozoic Mt-Isa Sequence. Nature 293(5830):284–286
Nichols RF (1984) Greenex A/S. Black Angel drilling. 1983 year end report. Internal report, Greenex A/S, 19 pp., 2 app., 6 plates. https://data.geus.dk/gg_detail/?cat=rap&id=24530. Accessed May 2022
Oliveira SB, Leach DL, Juliani C, Monteiro LVS, Johnson CA (2019) The Zn–Pb mineralization of Florida Canyon, an evaporite-related Mississippi Valley-type deposit in the Bongará district, northern Peru. Econ Geol 114:1621–1647
Oliveira SB, Juliani C, Monteiro LVS, Tassinari CCG (2020) Structural control and timing of evaporite-related Mississippi Valley-type Zn–Pb deposits in Pucará Group, northern central Peru Journal of South American. Earth Sciences 103:1–11

Oliveira SB, Johnson CA, Juliani C, Monteiro LVS, Leach DL, Caran MGN (2021) Geology and genesis of the shalipayco evaporite-related mississippi Valley-type Zn–Pb deposit, Central Peru: 3D Geological Modeling and C–O–S–Sr Isotope Constraints: Mineralium Deposita, 56: 1543–1562.

Olson RA (1984) Genesis of paleokarst and strata-bound zinc-lead sulfide deposits in a Proterozoic dolostone, northern Baffin Island. Canada Econ Geol 79:1056–1103

Ovchinnikova GV, Kuznetsov AB, Melezhik VA, Gorokhov IM, Vasileva IM, Gorokhovskii (2007) Pb-Pb age of Jatulian carbonate rocks: the Tulomozero Formation of southeast Karelia. Stratigr Geol Correl 15:359–372

Page RW, Jackson MJ, Krassay AA (2000) Constraining sequence stratigraphy in north Australian basins: SHRIMP U-Pb zircon geochronology between Mt Isa and McArthur River. Aust J Earth Sci 47(3):431–459

Page RW, Sweet IP (1998) Geochronology of basin phases in the western Mt Isa Inlier, and correlation with the McArthur Basin. Aust J Earth Sci 45:219–232

Partin CA, DeWolfe YM, Magee T (2021) Origin of sediment-hosted Pb-Zn mineralization in the Paleoproterozoic Mârmorilik and Qaarsukassak formations, Karrat Group, West Greenland. Ore Geol Rev 134:104164

Pedersen FD (1978) Report on geological field work 1978. Greenex A/S utilization and exploration concession Marmorilik district, West Greenland. Internal report, Greenex A/S, 79 pp, 1 map. https://data.geus.dk/gg_detail/?cat=rap&id=24533. Accessed May 2022

Pedersen FD (1980) Remobilization of the massive sulfide ore of the Black Angel Mine, Central West Greenland. Econ Geol 75:1022–1041

Pedersen FD (1981) Polyphase Deformation of the massive sulphide ore of the Black Angel Mine, Central West Greenland. Mineral Deposita 16:157–176

Pehrsson SJ, Eglington BM, Evans DA, Huston D, Reddy SM (2016) Metallogeny and its link to orogenic style during the Nuna supercontinent cycle. Geological Society, London, Special Publications 424(1):83–94

Pierre C, Rouchy JM (1988) Carbonate Replacements after sulfate evaporites in the Middle Miocene of Egypt. J Sediment Petrol 58(3):446–456

Pirajno F, Burlow RA (2009) The Magellan non-sulfide lead deposit, Yerrida and Earaheedy Basins,Western Australia. Geological Survey of Western Australia. Record 2009/4: 18

Planavsky NJ, Bekker A, Hofmann A, Owens JD, Lyons TW (2012) Sulfur record of rising and falling marine oxygen and sulfate levels during the Lomagundi event. Proc Natl Acad Sci USA 109(45):18300–18305

Planavsky NJ, Reinhard CT, Wang X, Thomson D, MCGoldrick P, Rainbird RH, Johnson TM, Fischer WW, Lyons TW (2014) Low Mid-Proterozoic atmospheric oxygen levels and the delayed rise of animals. Science 346:635–638

Plumb KA, Ahmad M, Wygralak AS (1980) Mid-Proterozoic basins of north Australian craton-Regional geology and mineralization. In Hughes, F.E. (ed), Geology of the mineral deposits of Australia and Papua New Guinea: Melbourne, Australasian Institute of Mining and Metallurgy: 881–902

Pope MC, Grotzinger JP (2003) Paleoproterozoic Stark Formation, Athapuscow Basin, Northwest Canada: Record of cratonic-scale salinity crisis. J Sed Res 73(2):280–295

Poulton SW, Bekker A, Cumming VM, Zerkle AL, Canfield DE, Johnston DT (2021) A 200-million-year delay in permanent atmospheric oxygenation. Nature 592(7853):232–236

Rickard DT, Zweifel H, Donnelly TH (1979) Sulfur isotope systematics in the Åsen Pyrite-Barite Deposits Skellefte District. Sweden Econ Geol 74:1060–1068

Rosa D, Dewolfe M, Guarnieri P, Kolb J, LaFlamme C, Partin C, Salehi S, Sørensen EV, Thaarup S, Thrane K, Zimmermann R (2017) Architecture and mineral potential of the Paleoproterozoic Karrat Group, West Greenland: results of the 2016 Season. Geological Survey of Denmark and Greenland Report, 2017/5, 112 p.

Rosa D, Bernstein S, Dewolfe M, Dziggel A, Grocott J, Guarnieri P, Kolb J, Partin C, Sørensen EV, Zimmermann R (2018) Architecture and mineral potential of the Paleoproterozoic Karrat Group, West Greenland: Results of the 2017 Season. Geological Survey of Denmark and Greenland Report, 2018/23, 102 p.

Ryan MJ, Escher JC (1999) Albitised gneisses in the area between Paakitsoq and Kangerluarsuk, north-east Disko Bugt, West Greenland. Geol Greenl Surv Bull 181:113–117

Sahoo SK, Planavsky NJ, Kendall B, Wang XQ, Shi XY, Scott C, Anbar AD, Lyons TW, Jiang GQ (2012) Ocean oxygenation in the wake of the Marinoan glaciation. Nature 489(7417):546–549

Sangster DF (1990) Mississippi Valley-type and sedex lead-zinc deposits: a comparative examination. Trans Instn Min Metall Sect B 99:B21–B42

Sanz-Rubio E, Sanchez-Moral S, Canaveras JC, Calvo JP, Rouchy JM (2001) Calcitization of Mg-Ca carbonate and Ca sulphate deposits in a continental Tertiary basin (Calatayud Basin, NE Spain). Sed Geol 140(1–2):123–142

Sarkar SC, Banerjee S (2004) Carbonate-hosted lead-zinc deposits of Zawar, Rajasthan, in the context of the world scenario. In: Deb M, Goodfellow WD (eds) Sediment-hosted lead-zinc sulphide deposits - attributes and models of some major deposits in India, Australia and Canada. Narosa Publishing House, New Delhi, pp 328–349

Sasaki A, Krouse HR (1969) Sulfur isotopes and the Pine Point lead-zinc mineralization: Econ. Geol 64:718–730

Schaefer MO, Gutzmer J, Beukes NJ, Greyling NL (2004) Mineral chemistry of sphalerite and galena from Pb-Zn mineralization hosted by the Transvaal Supergroup, in Griqualand West, South Africa. S Afr J Geol 107:341–354

Schröder S, Bekker A, Beukes NJ, Strauss H, van Niekerk HS (2008) Rise in seawater sulphate concentration associated with the Paleoproterozoic positive carbon isotope excursion: evidence from sulphate evaporites in the 2.2–2.1 Gyr shallow marine Lucknow Formation. South Africa Terra Nova 28:108–117

Scott C, Wing BA, Bekker A, Planavsky NJ, Medvedev P, Bates SM, Yun M, Lyons TW (2014) Pyrite multiple-sulfur isotope evidence for rapid expansion and contraction of the early Paleoproterozoic seawater sulfate reservoir. Earth Planet Sci Lett 389:95–104

Serdyuchenko DP (1975) Some Precambrian scapolite-bearing rocks evolved from evaporites. Lithos 8(1):1–7

Sergeev N, Burlow R, Tessalina S (2017) The Paroo Station Mine supergene lead deposits, Western Australia: geological and geochemical constraints. Ore Geol Rev 80:564–593

Stafford KW, Ulmer-Scholle D, Rosales-Lagarde L (2008) Hypogene Calcitization: evaporite diagenesis in the Western Delaware Basin. Carbonates Evaporites 23(2):89–103

St-Onge MR, van Gool JAM, Garde AA, Scott DJ (2009) Correlation of Archaean and Palaeoproterozoic units between northeastern Canada and western Greenland: constraining the pre-collisional upper plate accretionary history of the Trans-Hudson orogeny. In: Cawood PA and Kroner A (Eds) Earth Accretionary Systems in Space and Time. The Geological Society, London, Special Publications, 318: 193–235.

Taylor PN, Kalsbeek F (1990) Dating of metamorphism of Precambrian marbles: examples from Proterozoic mobile belts in Greenland. Chem Geol 86:21–28

Thode HG, Monster J (1965) Sulfur-isotope geochemistry of petroleum, evaporites, and ancient seas, fluids in subsurface environments. AAPG Mem 4:367–377

Thomassen B (1991) The Black Angel lead-zinc mine 1973–90. Rapp Grønl Geol Unders 152:46–50

Tompkins LA, Rayner MJ, Groves DI, Roche MT (1994) Evaporites; in situ sulfur source for rhythmically banded ore in the Cadjebut Mississipp Valley-type Zn-Pb deposit, Western Australia: Econ. Geol 89:467–492

Tran HT, Ansdell KM, Bethune KM, Ashton K, Hamilton MA (2008) Provenance and tectonic setting of Paleoproterozoic metasedimentary rocks along the eastern margin of Hearne craton: Constraints from SHRIMP geochronology, Wollaston Group, Saskatchewan. Canada Precambrian Research 167(1–2):171–185

Turner TC, Bekker A (2016) Thick sulfate evaporite accumulations marking a mid-Neoproterozoic oxygenation event (Ten Stone Formation, Northwest Territories, Canada). GSA Bull 128(1–2):203–222

Vearncombe JR, Dentith M, Doerling S, Reed A, Cooper R, Hart J, Muhling P, Windrim D, Woad G (1995) Regional- and prospect-scale fault controls on Mississippi Valley-type Zn-Pb mineralization at Blendevale, Canning basin, Western Australia. Econ Geol 90:181–186

Viets JG, Hofstra AH, Emsbo P, Kozlowski A (1996) The composition of fluid inclusions in ore and gangue minerals from Mississippi Valley-type Zn–Pb deposits of the Cracow–Silesia region of southern Poland: genetic and environmental implications. In: Gorecka E, Leach DL (eds) Carbonate-hosted zinc–lead deposits in the Silesian–Cracow area, Poland. Prace PIG, 154: 85–104.

Walford PC, Franklin JM (1982) The Anderson Lake Mine, Snow Lake, Manitoba. In: Precambrian Sulphide Deposits, HS Robinson memorial Volume, Hutchinson RW, Spence CD, Franklin JM, eds., Geological Association of Canada, Special Paper 25: 481–523.

Wallace MW, Hood AVS, Shuster A, Greig A, Planavsky NJ, Reed CP (2017) Oxygenation history of the Neoproterozoic to early Phanerozoic and the rise of land plants. Earth Planet Sci Lett 466:12–19

Walker RN, Muir MD, Diver WL, Williams N, Wilkins N (1977) Evidence of major sulphate evaporite deposits in the Proterozoic McArthur Group, Northern Territory, Australia. Nature 265:526–529

Walker RN, Gulson B, Smith J (1983) The Coxco deposit-A Proterozoic Mississippi Valley-type deposit in the McArthur River District, Northern Territory. Australia Econ Geol 78:214–249

Wang C, Lechte MA, Reinhard CT, Asael D, Cole DB, Halverson GP, Porter SM, Galil N, Halevy I, Rainbird RH, Lyons TW, Planavsky NJ (2022) Strong evidence for a weakly oxygenated ocean–atmosphere system during the Proterozoic. PNAS 119:e2116101119

Warren JK (2016) Evaporites: a geological compendium Berlin. Springer, Germany, p 1813

Warren JK, Kempton RH (1997) Evaporite sedimentology and the origin of evaporite-associated Mississippi Valley-type sulfides in the Cadjebut mine area Lennard shelf, Canning basin, Western Australia. Society for Sedimentary Geology, Special Publication 57:183–205

Whelan JF, Rye RO, de Lorraine W, Ohmoto H (1990) Isotopic geochemistry of the mid-Proterozoic evaporite basin. Balmat, New York: American Journal of Science 290:396–424

Williams JJ, Mills BJW, Lenton TM (2019) A tectonically driven Ediacaran oxygenation event. Nat Commun 10:2690

Wilton DHC, Archibald SM, Hussey AM, Butler RW (1994). Metallogeny of the Ramah Group: discovery of a new Pb–Zn exploration target, northern Labrador. Newfoundland Department of Energy and Mines Current Research 94–1:415–428

Yao W, Wortmann UG, Paytan A (2019) Sulfur isotopes—use for stratigraphy during times of rapid perturbations. Stratigraphy & Timescales, 4, Chapter 1: 33 p.

Zentmyer RA, Pufahl PK, James NP, Hiatt EE (2011) Dolomitization on an evaporitic Paleoproterozoic ramp: widespread synsedimentary dolomite in the Denault Formation, Labrador Trough. Canada Sedimentary Geology 238(1–2):116–131

Zhao Z, Leach D, Wei J, Liang S, Pfaff K (2021) Origin of the Xitieshan Pb-Zn deposit, Qinghai, China: evidence from petrography and S-C-O-Sr isotope geochemistry. Ore Geol Rev 139:104429